

Bulk Metallic Glasses with Functional Physical Properties

By W. H. Wang*

In this review, we report on the formation of a variety of novel, metallic, glassy materials that might well have applications as functional materials. The metallic glasses, with excellent glass-forming ability, display many fascinating properties and features such as excellent wave-absorption ability, exceptionally low glass-transition temperatures ($\sim 35\text{--}60^\circ\text{C}$) approaching room temperature, ultralow elastic moduli comparable to that of human bone, high elasticity and high strength, superplasticity and polymer-like thermoplastic formability near room temperature, an excellent magnetocaloric effect, hard magnetism and tunable magnetic properties, heavy-fermion behavior, superhydrophobicity and superoleophobicity, and polyamorphism, all of which are of interest not only for basic research but also for technological applications. A strategy based on elastic-moduli correlations for fabrication of bulk metallic glasses (BMGs) with controllable properties is presented. The work has implications in the search for novel metallic glasses with unique functional properties, for advancing our understanding of the nature and formation of glasses, and for extending the applications of the materials.

Metallic glasses have been vigorously studied since the discovery of bulk metallic glasses (BMGs). Now, the study and development of BMGs are at the cutting edge of metal research because the materials open new opportunities for both fundamental studies and commercial applications.^[1–6] The initial interest and purpose for developing BMGs are in engineering applications because of their attractive mechanical properties, such as high strength, high elasticity and near-net-shape processing.^[1–7] Extensive work has been done in exploring new glassy alloys with excellent mechanical properties.^[7–15] Many interesting results in basic research and some applications have been achieved, while many issues remain unresolved.^[1–15] Three main flaws of BMGs restrict their widespread applications: the plasticity of most BMGs at room temperature (RT) is depressively low, and in uniaxial tension their plastic strain is near zero.^[1–6]

1. Introduction

A new, glassy material with unique properties could have an important impact on the scientific community and even daily life.^[1] For example, oxide glasses are widely used in scientific instruments, bottles, window panes, and many other items that improve our everyday life.^[1] Glassy polymers are a sort of glass applied widely because they exhibit a low glass-transition temperature T_g , a stable, supercooled-liquid region for formability, and low cost. Metallic glasses are comparative newcomers in the glassy family,^[1–6] and are currently of fundamental interest and technological importance worldwide because they offer attractive benefits, combining some of the desirable mechanical, magnetic, and chemical properties of crystalline alloys and the formability of oxide glasses. On the other hand, metallic glasses with a close-packed Bernal structure provide a model system for studying the challenging issues of the glass's nature and its supercooled-liquid state.^[1] Many important issues could be addressed if stable, metallic, supercooled liquids or new metallic glasses could be created.^[1–6]

Even under relatively stable compression, the plastic strain remains very limited ($\sim 2\%$) for most BMGs, due to shear localization and work-softening. The lack of plasticity makes BMGs prone to catastrophic failure in load-bearing conditions which hinder their application as a structural material.^[1–6] Another major issue is the limited glass-forming ability (GFA) of most known BMGs, which are based on engineering metals such as Mg, Fe, Zr, Cu, Ni, Co, Al, and Ti; their critical size, even under laboratory conditions, is normally less than 10 mm, which restricts large-scale industry production and processing.^[1–6] BMGs with an oxide-glass-like GFA are indeed difficult to come by. The third issue is that the GFA of most BMGs is sensitive to oxygen and impurities, and therefore, melting and processing have to be performed under vacuum or inert-gas-protected conditions, boosting the material cost and practical difficulties for industrial production. Therefore, it would be remarkable if BMGs with unique properties like those of crystalline materials could be used as functional materials. This would mean that the applications of BMGs could be substantially extended and their intrinsic problems for applications such as brittleness, limited GFA and cost could be much mitigated.

In this paper, we systematically review the formation, characteristics, and unique mechanical and physical properties of various BMGs. The many interesting phenomena and unique properties and features of these BMGs can advance our understanding of the nature of glass, assist in the search for

[*] Prof. W. H. Wang
Institute of Physics, Chinese Academy of Sciences
Beijing 100190, (PR China)
E-mail: whw@aphy.iphy.ac.cn

DOI: 10.1002/adma.200901053

new BMGs and promote their commercial applications. Rare-earth-based crystalline functional materials are ubiquitous in applications from magnetic devices to space flight. We give, therefore, special attention to discussing glass formation in rare-earth-element-based alloys according to the elastic-modulus rule in combination with classic glass-forming criteria.^[15] The elastic, electric and magnetic properties are addressed for a series of new Y-, Sc-, La-, Ce-, Nd-, Pr-, Gd-, Sm-, Tb-, Dy-, Ho-, Er-, Yb-, Tm- and Lu-based BMGs with unique electronic structures, good GFA and high thermal stability.^[15–56] The review is organized in four sections. The first is a brief introduction. The second section introduces the formation and design of BMG materials according to elastic-moduli correlations. The third section is a comprehensive review of the unique physical, elastic, and mechanical properties and features of BMGs, and the physical details underlying the properties of BMGs are also discussed. The last section is an overview of the significance of BMG materials with functional physical properties, both in technological applications and in basic research, and the outlook for future study in this topic.

2. Formation and Design of BMGs based on their Elastic Moduli

A major challenge in the field of metallic-glassy materials is to explore new alloys or compositions with excellent glass-forming ability in a simple operation such as copper model casting.^[4] Quite a number of criteria have been proposed to predict the GFA of alloys, based on their thermodynamic quantities, and kinetic constraints on crystal nucleation and/or growth in a BMG's formation,^[57–62] and these criteria have played an important role in the exploration of novel compositions and systems of metallic glasses. However, none of these criteria have been established to be sufficiently robust and predictive to be considered as necessary and sufficient for bulk-glass formation. In addition, none of them can be used to control the properties of the formed metallic glasses, and the development of new metallic glass in practice has always been "hit or miss" as to whether the resulting glass has excellent GFA or is excellent in some properties. We propose that the elastic moduli of BMGs, which have correlations with the glass features, mechanical and physical properties and even liquid fragility, give useful directions in general for exploring BMGs with desirable properties, although the theoretical and physical reasons for the correlations are to be further clarified. Elastic-moduli correlations could also assist in understanding longstanding issues of glass formation and their nature, and simulate the work of theorists.

2.1. Elastic-Moduli Correlations and their Role in the Design of BMGs with Controllable Properties

The idea that instantaneous (high-frequency) elastic moduli are the key physical quantities controlling the main thermodynamic and kinetic properties of supercooled liquids and glasses is currently considered to be one of the most-promising approaches in the physics of glassy materials.^[15,63–67] Glass formation from the solidification of a liquid, and the mechanical deformation, relaxation and stability of glasses can be treated as a change of



Wei Hua Wang is a professor of the Institute of Physics, Chinese Academy of Sciences at Beijing, China. His research focuses on the formation, structure, physical properties and glass transition in metallic glasses. He earned his Ph.D. degree in condensed-matter physics at the Chinese Academy of Sciences in 1993, and was Humboldt fellow in 1995–1997. He has published more than 150 papers in international journals.

their different configurations or flow, and the flow can be modelled as activated hopping between inherent states in the potential-energy landscape via crossing over energy barriers. The energy barriers of the flow or both the Newtonian and non-Newtonian viscosities of the metallic-glass-forming liquids over a broad range of rheological behavior correlate well with the instantaneous moduli.^[15,63–66] Experimental data of high-frequency, ultrasonic measurements confirm the validity of the proposed treatment.^[15,63–66] The variation in shear modulus induced either by thermal excitation or mechanical deformation can be correlated to variations in the measured stored enthalpy or, equivalently, to the configurational potential energy of the liquid. Recently, some plausible correlations between the thermodynamic, kinetic, physical and elastic properties of BMGs, such as between fragility and the Poisson ratio, between T_g and the elastic moduli, between T_g and the Debye temperature, between plasticity and the Poisson ratio, and between the Boson peak and the elastic moduli, have indeed been found.^[15,63–74] On the one hand, these elastic correlations confirm the elastic model for understanding the glass and the supercooled-liquid state. On the other hand, the correlations can be used to develop new metallic glasses with desirable properties. The elastic-moduli criteria can be described as: the elastic moduli, M , correlate with the glass formation, thermal stability, and the mechanical and some of the physical properties of BMGs. Furthermore, the M of BMGs show a good correlation with a weighted average of the elastic constants M_i of the constituent elements as:^[15] $M^{-1} = \sum f_i \cdot M_i^{-1}$, where f_i denotes the atomic percentage of the constituent. The results indicate that some features, glass formation and properties of a BMG depend strongly on the *elastic moduli* of its components. Therefore, the glass formation and some of the features and properties of a glass-forming alloy can be predicted by its related elastic moduli through a selection of components with suitable elastic moduli. The established correlations, associated with the elastic moduli, and the fact that the moduli of the glasses scale with those of their elemental components provide useful guidelines for the development of BMGs with desirable properties (such as mechanical, thermal, and elastic properties) by the selection of components with suitable elastic moduli. Combining the existing, empirical criteria,^[1] the elastic-moduli criteria can efficiently improve the search for interesting BMGs, especially BMGs with tunable properties.

Some of the behaviors and properties of BMGs can be sensitively modulated by minor addition or microalloying of elements with specific properties.^[6,75] The microalloying techni-

que, in particular, the microalloying of rare-earth elements with plentiful and unique physical properties, plays an effective and important role in the design, fabrication and property improvement of BMGs.^[6] For example, the addition of as little as 0.5 at % of Gd (with 4*f* electrons) can dramatically change the correlations among the electrons in CuZr- and MgCu-based BMGs, and induce unique magnetic and electric properties;^[76] minor addition of carbon and carbon nanotubes can markedly improve the mechanical and acoustic properties of BMGs.^[75,77] The minor-addition method combined with elastic-moduli correlations can effectively be used to search for BMGs with controllable properties. Therefore, the general method for the development of BMGs with desired properties is first to select a proper, single, base element according to the elastic-moduli correlations and then to match the base element to other glass-forming constituents. The minor addition method can be used to further improve the GFA and properties. The optimum contents of the additions are normally found to be in a very-narrow composition range. Thus, the selection of suitable additional materials and the method of pinpointing the optimal fraction of the additional material are important.

2.2 Formation of Rare-Earth-Based BMGs with Tunable Properties based on the Elastic-Moduli Criteria

A family of rare-earth (RE)-based BMGs with controllable properties actually was developed based on the elastic-moduli criteria.^[15] For example, to develop rare-earth-based BMGs with higher thermal stability and elastic moduli, we selected Er, Tm and Sc as base elements due to their higher elastic moduli (e.g., for Er: Young's modulus, $E = 70$ GPa; bulk modulus, $K = 44$ GPa; and shear modulus $G = 28$ GPa^[15]) among the rare-earth family. Er (Sc, Tm)-Co alloys were prepared first because of the large, negative enthalpy of formation between the RE and the Co. With the minor addition of Al and Y, the GFA of the Er-Co alloy can be greatly improved, and a new family of Er-based BMGs was then developed.^[13] In a similar way, we fabricated a series of rare-earth-based BMGs that offer unique physical properties.^[15-56] The rare-earth elements in the largest chemically coherent group in the periodic table possess a complicated and specific electric and magnetic structure. So Y, Sc-, La-, Ce-, Nd-, Pr-, Gd-, Sm-, Tb-, Dy-, Ho-, Er-, Yb-, Tm- and Lu-based BMGs can be fabricated into the completed glass in bulk form. A critical diameter reaching 30 mm for fully glassy, La-based alloy rods, and Ce-, Y-, Nd-, and Er-based BMGs with thicknesses exceeding 1 cm have been reported. Figure 1a shows a picture of a fully glassy, Er-based alloy ($\text{Er}_{36}\text{Al}_{24}\text{Co}_{20}\text{Y}_{20}$ BMG) with its largest critical diameter exceeding 1 cm in cylinder. Table 1 shows the typical compositions of these RE-based BMGs. It is noted that the formation of RE-based BMGs does not follow the predictions of the classical criteria.^[57-62]

For RE-based BMGs, a multibase formation strategy exists to fabricate alloys with controlled properties. RE-based BMGs can usually be made based on two or more Res, owing to the physical coherency and comparability of the REs, and the ratio of the REs can be arbitrarily changed in a large composition range (in this sense we call them multibases), which is not ordinary for

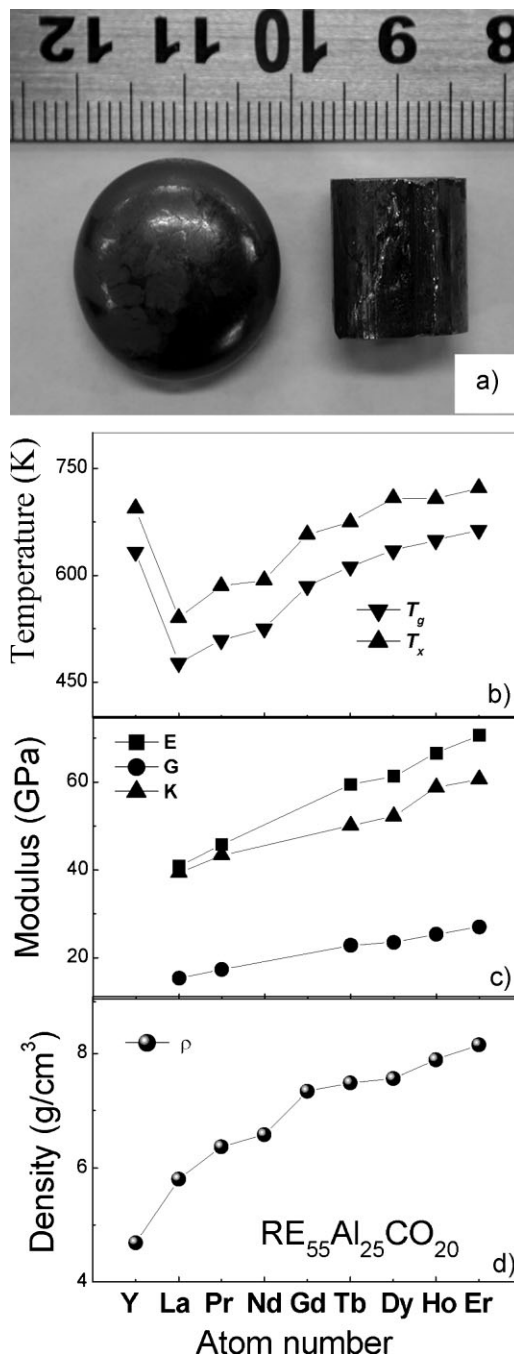


Figure 1. a) A picture of an $\text{Er}_{36}\text{Al}_{24}\text{Co}_{20}\text{Y}_{20}$ BMG with its largest critical diameter exceeding 1 cm in cylinder, which can be cast fully glassy. b) The dependence of T_g and T_x on the atomic number of the RE, for as-cast $\text{RE}_{55}\text{Al}_{25}\text{Co}_{20}$ BMGs. c) The dependence of the elastic moduli E , G and K on the atomic number of the RE, for as-cast $\text{RE}_{55}\text{Al}_{25}\text{Co}_{20}$ BMGs. d) The dependence of the density on the atomic number of the RE, for as-cast $\text{RE}_{55}\text{Al}_{25}\text{Co}_{20}$ BMGs. Figure 1b–d are reproduced with permission from ref.^[28]; copyright 2008, Elsevier.

transition-element families such as Zr-, Fe-, Co-, Ni- and Cu-based BMGs. Even mischmetal (including La, Ce, Pr, Nd, etc.)-based BMGs with modulated thermoplastic and mechanical properties can be formed readily.^[21] It has been found that the

Table 1. The typical compositions of RE-based BMG systems.^[15–56]

Element	Typical BMGs system
Sc	Sc-Al-Co-Y
Y	Y-Sc-Al-Co, Y-Al-Co(Ni)
La	La-Al-Ni-Cu, La-Al-Co(Ni)
Pr	Pr-Fe-Al, Pr-Al-M-N (M, N = Fe, Cu, Ni, Co)
Ce	Ce-Al-M [M = Cu, Co, Ni, Ce-Al-Cu-X (X = Co, Nb, B, etc.)]
Nd	Nd-Al-Fe, Nd-Al-M-N (M, N = Fe, Cu, Ni, Co)
Sm	Sm-Al-Co(Ni), Sm-Al-Co-X (X = Y, Nb)
Gd	Gd-Al-Co(Fe, Ni), Gd-Al-Ni-Cu(Co), Gd-Y-Al-Co(Ni)
Tb	Tb-Al-Co, Tb-Y-Al-Co
Dy	Dy-Al-Co(Ni), Dy-Y-Al-Co
Ho	Ho-Al-Co, Ho-Y(Zr)-Al-Co
Er	Er-Al-Co(Ni), Er-Y-Al-Co(Ni, Fe)
Tm	Tm-Al-Co, Tm-Y(Zr)-Al-Co
Yb	Yb-Zn-Mg, Yb-Zn-Mg-Cu
Lu	Lu-Al-Co, Lu-Y(Zr)-Al-Co

liquid fragility, and the elastic and electric properties of LaCe-based BMGs can be modulated by gradually changing the ratio of the two bases, La and Ce.^[43]

The GFA and properties of RE-based BMGs are extremely sensitive to minor additions of elements. For instance, in Ce-based BMGs, a minor addition of 0.2% Co can dramatically increase the critical diameter from 2 mm to at least 8 mm.^[22] Note that Co has an atomic size similar to that of Cu, suggesting that the “confusion principle” and the atom-size effect alone cannot account for this subtle influence. A distinct, relative “fragile” to “strong” transition has been observed in the BMG by microalloying with 1% Co.^[22] This means that the minor addition has a salient impact on the dynamics and stability of the liquid through microstructural changes. The acoustic velocities, the Debye temperature and the elastic moduli also show an abrupt change (relative to the matrix alloy) for the alloy with addition of 0.2% Co. Such large changes of these properties suggest that the alloy falls into a more-dense packing structure with significant changes of the short-range order due to the minute Co addition. A nuclear-magnetic resonance experiment shows that the symmetry around the Al sites is enhanced significantly upon the addition of Co, as revealed by the decreasing quadrupole frequency, measured by ²⁷Al NMR spectroscopy.^[67] The minor addition can stabilize the liquid phase, suppress the crystallization kinetics, and enhance the glass formation of the BMGs. The process is accompanied by a stronger tendency for short-range ordering and a stronger liquid behavior.

The properties of a BMG depend very much on its base element. Therefore, the selection of the RE bases directly results in various, attractive, mechanical, chemical, magnetic and other properties. The versatile and well-regulated physical and chemical properties of REs in the lanthanum family bring forth peculiar features for RE-based BMGs. A series of RE-Al-Co(Ni)-Y(Zr) BMGs (RE = La, Pr, Gd, Tb, Dy, Ho, Er, Tm, Lu) with tunable properties, such as magnetic and mechanical properties, have been successfully fabricated by means of the elastic-modulus rule.^[25–29] Their T_g and T_x (T_x = crystallization temperature) cover large ranges of ~341–678 K and ~377–760 K, respectively. The T_g

can be as low as near room temperature (RT), and as high as those of Zr-based BMGs. Importantly, these large ranges of properties can be well controlled and tuned by changing the composition, based on elastic-moduli correlations. Such an example is shown in Figure 1 for the case of the RE₅₅Al₂₅Co₂₀ series. The availability of RE-based BMGs with well-regulated mechanical and physical properties, via the multibase formation strategy, can assist in understanding the correlations among the properties and elastic constants, and permit a better understanding of the electric and magnetic properties. Tunable and improved thermoplastic properties, hard magnetic properties and the magnetocaloric effect of BMGs could extend the applications of metallic glasses as functional materials.

3. Unique Properties and Features of BMGs

The specificity and versatility of crystalline alloys with functional properties have given them a high level of technological, environmental, and economic importance. For instance, samarium-cobalt and iron-neodymium-boron alloys are well known as extremely stable magnets with high remanence and coercive field strengths. These magnets form an integral part of hard-disk drives, electric motors, and compact headphones; transition-metal-RE films are well known for their magnetic recording and memory applications. As relative newcomers, BMGs are also found to display many unique and attractive physical and chemical properties and features. It is expected that, as more and more new BMGs systems with unique physical properties are developed, the materials would become promising for functional applications.

3.1. Hard Magnetic Properties of Nd(Pr, Sm)-Based BMGs

Fe-rich Nd(Pr, Sm)-based BMGs have hard magnetic properties at room temperature.^[16,40,42] Furthermore, the coercivity of ferromagnetic BMGs depends strongly on the cooling rate or the preparation method, indicating a subtle relationship between the structural characteristics and the magnetic properties. The coercivity of an as-cast Nd₆₀Fe₃₀Al₁₀ BMG is about 277 kA m⁻¹ at RT, whereas the same melt-spun ribbons exhibit softer magnetic behavior with a coercivity, H_c of only several kA m⁻¹.^[78] Figure 2 shows the M–H hysteresis loops for Nd₆₀Al₁₀Fe₂₀Co₁₀ metallic glass for different melt spinning rates; one can see the marked change of coercivity versus quenching rate. The strong dependence of the magnetic features on the microstructure can be clearly seen from the fact that the hard magnetic properties do not change significantly with annealing around T_g but usually disappear when the samples are completely crystallized.^[16,40,42] It is generally accepted that the high coercivity is attributable to a variety of different, metastable phases (or clusters) and microstructures.^[16,40,42,78–82] The nanoscale clusters consisting of Nd and/or transition metals are generally observed in Nd(Pr)-based glasses by high-resolution transmission electron microscopy (TEM), Mössbauer spectroscopy, magnetic and resistance measurements, and isothermal-calorimetry investigations.^[16,40,42,78–82] Schneider et al.^[78–79] attributed the intrinsic

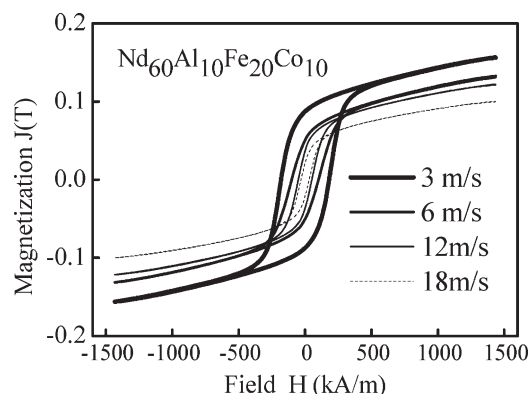


Figure 2. The M - H hysteresis loops for $\text{Nd}_{60}\text{Al}_{10}\text{Fe}_{20}\text{Co}_{10}$ ribbons melt-spun at different speeds.

composite structure to a phase-separation process taking place in the melt. Sun et al.^[83] showed an existence of two amorphous magnetic phases in melt-spun $\text{Nd}_{60-x}\text{Y}_x\text{Fe}_{30}\text{Al}_{10}$ ($x = 0, 10, 30$) ribbons. Experimentally, the microstructure of Nd-Fe-based glasses is sensitive to the preparation conditions, which usually lead to the different microstructures that have been observed for the same compositions by different authors. Based on the cluster model of the Nd-Fe magnetic system, the hard magnetic behavior of these alloys is regarded as being due to the magnetic-exchange-coupling interaction among the magnetic clusters that have a large, random anisotropy.^[16] The large, random magnetic anisotropy (RMA) constrains the vector of the magnetic moments in the orientation of the local anisotropy. Hard magnetic properties can be expected through the exchange coupling among the clusters, when the cluster size matches the single domain size. The presence of the exchange-coupling interaction between short-scale, ordered, magnetic atomic clusters is confirmed by magnetic-force images in a $\text{Nd}_{60}\text{Al}_{10}\text{Fe}_{20}\text{Co}_{10}$ BMG.^[16] Besides the paramagnetic phases, the grain boundaries, surfaces and magnetic inhomogeneities can play an important role as pinning sites of the domain walls. The strong domain-wall-pinning mechanism (the pinning criterion is satisfied when $a \gg \delta^2$, where a is the lateral area of a single pin and δ is the wall width^[83]) has been well proven in these Nd-based alloys from the temperature dependence of the coercivity.^[16,78-80] This is because the condition of large impediments and narrow domain walls (small δ) are easily favored by the inhomogeneous structures and the large RMA in Nd-based alloys. Generally, the exchange-coupling interactions of the magnetic clusters with the RMA determine the coercivity in the high-temperature region. With decreasing temperature, the coercivity increases, indicating that the thermally activated pinning mechanisms gradually dominate the enhancement of the coercivity, until the pinning clusters become magnetically ordered. Since the exchange coupling, the large magnetic anisotropy and the pinning mechanism are all sensitive to the morphology and composition of the various clusters, the magnetic properties of these BMGs are strongly dependent on the cooling rate. For bulk samples fabricated with lower cooling rates, the atoms have more time to rearrange and diffuse for lower energetic configurations, and thus a variety of atomic clusters

with a certain degree of short-range or medium-range order may be formed. As the number and size of the clusters increase, the exchange couplings are strengthened and pinning centers form more easily. Therefore, the magnetic properties of these BMGs can be tuned by monitoring their microstructure through processing, annealing, relaxation and partial crystallization.

3.2. The Magnetocaloric Effect in RE-Based BMGs

Recently, there has been increasing interest in materials with applications as magnetic refrigerants:^[84-87] we found RE-based BMGs to be promising candidates.^[34-35,51] Figure 3a shows the typical temperature dependence of the magnetization for $\text{Gd}_{51}\text{Al}_{24}\text{Co}_{20}\text{Zr}_4\text{Nb}_1$ and $\text{Gd}_{55}\text{Ni}_{25}\text{Al}_{20}$ BMGs under 200 Oe, exhibiting a sharp magnetization change at the ordering temperature. Figure 3b shows that, at low temperature, Ho-, Dy-, Tb-, Er-based BMGs all show spin-glass-like behavior with obvious hysteresis, indicating that these alloys are harder magnetic than the Gd-based BMGs. The Ho-, Dy-, Tb- and Er-based BMGs possess moderate or strong random magnetic

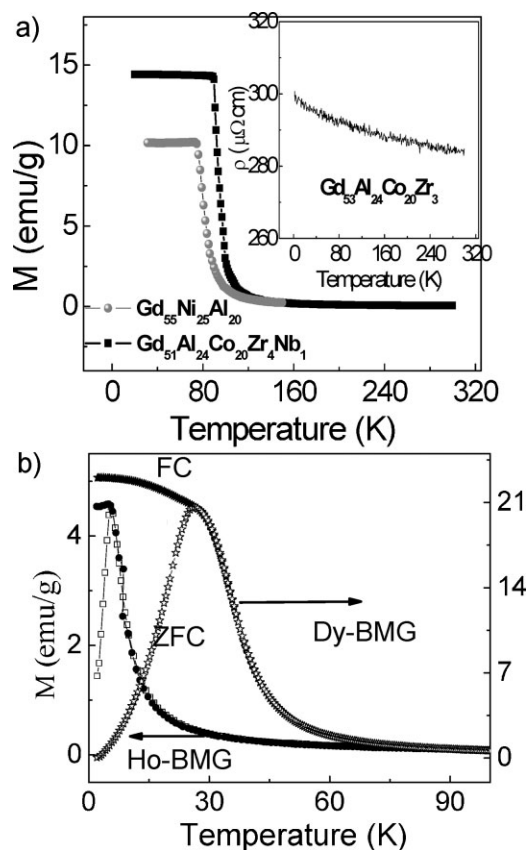


Figure 3. a) Temperature dependence of the magnetization under 200 Oe for $\text{Gd}_{51}\text{Al}_{24}\text{Co}_{20}\text{Zr}_4\text{Nb}_1$ and $\text{Gd}_{55}\text{Ni}_{25}\text{Al}_{20}$ BMGs. The inset shows the electric resistivity of $\text{Gd}_{53}\text{Al}_{24}\text{Co}_{20}\text{Zr}_3$ BMG. b) Temperature dependence of ZFC (open plots) and FC (filled plots) magnetization under 500 Oe for $\text{Dy}_{50}\text{Gd}_7\text{Al}_{23}\text{Co}_{20}$ and under 200 Oe for $\text{Ho}_{30}\text{Y}_{26}\text{Al}_{24}\text{Co}_{20}$. Reproduced with permission from ref.^[33]; copyright 2007, American Institute of Physics.

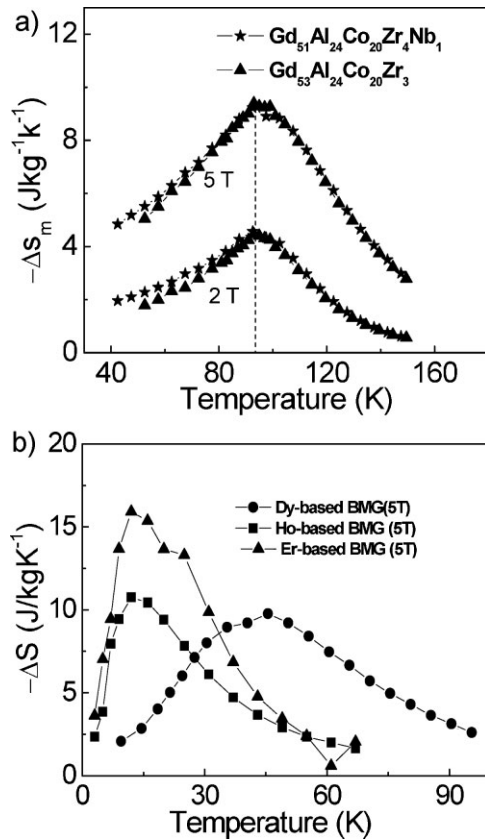


Figure 4. a) Magnetic-entropy changes for the as-cast $\text{Gd}_{51}\text{Al}_{24}\text{Co}_{20}\text{Zr}_4\text{Nb}_1$ and $\text{Gd}_{53}\text{Al}_{24}\text{Co}_{20}\text{Zr}_3$ BMGs. b) Magnetic-entropy changes for the as-cast $\text{Ho}_{30}\text{Y}_{26}\text{Al}_{24}\text{Co}_{20}$, $\text{Dy}_{50}\text{Gd}_7\text{Al}_{23}\text{Co}_{20}$ and $\text{Er}_{50}\text{Al}_{24}\text{Co}_{20}\text{Y}_6$ BMGs.

anisotropy (RMA) resulting in a lack of long-range ferromagnetic order and then the spin-glass behavior. However, near and above T_f or T_B (freezing temperature for spin-glass or block temperature for super-paramagnetism), no magnetic hysteresis is observed in the paramagnetic (super-paramagnetic) region. Figure 4a shows the magnetic-entropy change, $-\Delta S_m$, of typical Gd-based BMGs. For all of the samples, the position of the maximum of $-\Delta S_m$ was in the vicinity of the transition temperature, and the peak values of $-\Delta S_m$ were 9.40 $\text{J kg}^{-1} \text{K}^{-1}$ at 93 K, and 9.23 $\text{J kg}^{-1} \text{K}^{-1}$ at 92.5 K for $\text{Gd}_{53}\text{Al}_{24}\text{Co}_{20}\text{Zr}_3$ and $\text{Gd}_{51}\text{Al}_{24}\text{Co}_{20}\text{Zr}_4\text{Nb}_1$, respectively. In addition to the little magnetic hysteresis in the whole temperature range investigated, it is worth noting that the large value of $-\Delta S_m$ covers a much-broader temperature range than that of most crystalline materials.^[34–35] This directly results in an increased refrigerant capacity (RC) (the RC is determined by numerically integrating the area under the $\Delta S_m - T$ curve, using the temperatures at half-maximum of the peak as the integration limits) of 590 and 651 J kg^{-1} for $\text{Gd}_{53}\text{Al}_{24}\text{Co}_{20}\text{Zr}_3$ and $\text{Gd}_{51}\text{Al}_{24}\text{Co}_{20}\text{Zr}_4\text{Nb}_1$, respectively, which are much larger than those of crystalline refrigerants of $\text{Gd}_5\text{Si}_2\text{Ge}_2$ (305 J kg^{-1}) and $\text{Gd}_5\text{Si}_2\text{Ge}_{1.9}\text{Fe}_{0.1}$ (360 J kg^{-1}) alloys. The better RC, favored by practical usage in the Ericsson cycle, associates with the large magnetic moment of the alloys and their amorphous structure,

which extends the large magnetocaloric effect (MCE) to a wider temperature range. Figure 4b shows that the maxima of $-\Delta S_m$ for Dy-, Ho- and Er-based BMGs are comparable to or even larger than those of intermetallic alloys such as DyAl_2 , DyNi_2 , $\text{Dy}_{1-x}\text{Er}_x\text{Al}_2$ and $\text{Tb}_x\text{Y}_{1-x}\text{Al}_2$.^[88–89] Recently, more compositions in Gd-, Dy-, Er-, Ho-based BMGs with large MCE have also been found.^[90–93] The MCE of BMGs and other materials are presented in Table 2 for comparison. RE-based BMGs have the advantages of having a tailorable ordering temperature, higher electrical resistivity and thus smaller eddy-current heating, and high corrosion resistance. Compared with the glass ribbons, these bulk specimens particularly possess such advantages as low fabrication cost, outstanding mechanical properties and a large, supercooled-liquid region convenient for heat treatment and processing.

The aging and crystallization of BMGs have obvious impacts on their MCE, indicating the MCE is sensitive to their microstructure. An aging BMG sample was annealed at 300 °C ($T_g = 325$ °C) for 30 hrs, a fully crystallized sample was annealed at 650 °C for 5 hrs and two partially crystallized samples were annealed at 340 °C for 1 h and 430 °C for 1 h. In contrast to the sharp transition of the as-cast BMG near T_c , the magnetic transition is smeared out obviously for all of the treated samples, as shown in Figure 5a. After a long-time aging below T_g , the $-\Delta S_m$ reduces and the cusp also moves to lower temperature (Fig. 5b). The reduction is associated with atom and stress relaxation to a more-stable state, accompanied with a rearrangement of the atoms and an increase of the size of the nanoscale clusters. Similarly, the crystallization, partially or fully, always results in a remarkable reduction of $-\Delta S_m$. Interestingly, the partial devitrification of BMGs with nanocrystalline grains embedded in an amorphous matrix results in an almost-constant or table-like (see Fig. 5b) and relatively high magnetic-entropy change over a large temperature range. This favors practical application in the Ericsson cycle, in which ideal magnetic refrigerants with a constant magnetic-entropy change through the thermodynamic-cycle range are needed. Usually, multilayered structure materials are designed to meet this requirement,^[94] where ferromagnetic materials with varying Curie temperature are layered or sintered. Compared with the method of using layered or sintered composites, the crystallization method has the advantage of convenience and makes the construction of an active magnetic regenerator much simpler.

The effect of minor alloying on the MCE has been investigated. Figure 6a shows the magnetic-entropy change of these alloys. The alloying effects of Ce, Er and Cr only tune the position of the peak of $-\Delta S_m$ without changing the peak value and the RC of the alloy. The slight reduction of the peak value of $-\Delta S_m$ when adding minor amounts of the element boron is due to the few crystalline phases in the amorphous matrix, similar to the partial-crystallization effect. Minor alloying has a delicate influence on the MCE and can also be a useful tool to tune the working temperature.

The heavy RE-based BMGs alloys exhibit a large MCE over a relatively wider temperature range, compared with many crystalline materials. A comparison of the magnetic-entropy change among RE-based BMGs and other materials is shown in Figure 6b and Table 2. It is noted that $\text{RE}_1\text{RE}_2\text{-TM}$ series (RE = heavy rare-earth element, TM = transition metal) BMGs

Table 2. Magnetic entropy and related parameters for BMGs and other materials. The *a*, *c*, and *a + c* stand for the amorphous, crystalline and mixture of crystalline phases and amorphous phase, respectively. The refrigerant-capacity values are calculated using the same method.^[33]

Material	Structure	Applied field [T]	Peak of ΔS_m [J kg ⁻¹ K ⁻¹]	Transition temperature [K]	Refrigerant capacity [J kg ⁻¹]
Gd ₅₃ Al ₂₄ Co ₂₀ Zr ₃	<i>a</i>	5	9.4	93	590
Gd ₅₅ Ni ₂₅ Al ₂₀	<i>a</i>	5	9.76	79	–
Gd ₅₁ Al ₂₄ Co ₂₀ Ce ₅	<i>a</i>	5	8.85	81	679
Gd ₅₁ Al ₂₄ Co ₂₀ Nb ₁ Cr ₄	<i>a</i>	5	9.48	100	611
Gd ₅₁ Al ₂₄ Co ₂₀ Nb ₁ B ₄	<i>a + c</i>	5	7.98	74–90	504
Gd ₄₈ Al ₂₅ Co ₂₀ Zr ₃ Er ₄	<i>a</i>	5	9.41	84	647
Gd ₅₁ Al ₂₄ Co ₂₀ Zr ₄ Nb ₁	<i>a</i>	5	9.23	91	651
Gd ₃₃ Er ₂₂ Al ₂₅ Co ₂₀	<i>a</i>	5	9.47	52	574
Gd ₃₀ Al ₂₅ Co ₂₀ Y ₂₀ Zr ₅	<i>a</i>	5	7.64	37	413
Ho ₃₀ Y ₂₆ Al ₂₄ Co ₂₀	<i>a</i>	5	10.76	5.5	241
Dy ₅₀ Gd ₇ Al ₂₃ Co ₂₀	<i>a</i>	5	9.77	26	290
Er ₅₀ Al ₂₄ Co ₂₀ Y ₆	<i>a</i>	5	15.91	8	423
(Er _{0.7} Ho _{0.2} Dy _{0.1}) ₅₅ Ni ₂₅ Al ₂₀	<i>a</i>	5	14.02	3	277
Tb ₃₆ Y ₂₀ Al ₂₄ Co ₂₀	<i>a + c</i>	5	5.60	30	–
Gd ₆₀ Co ₂₆ Al ₁₄	<i>a</i>	5	10.1	79	557
Gd ₃₆ Er ₂₀ Al ₂₄ Co ₂₀	<i>a</i>	5	13.86	–	474
Gd ₃₆ Y ₂₀ Al ₂₄ Co ₂₀	<i>a</i>	5	7.76	–	459
Gd ₆₀ Fe ₃₀ Al ₁₀	<i>a + c</i>	5	3.53	200	754
Gd ₇₀ Fe ₁₅ Al ₁₅	<i>a + c</i>	5	6.12	170	764
Gd	<i>c</i>	5	9.8	293	–
Gd ₅ Si ₂ Ge ₂	<i>c</i>	5	18.6	276	306
Gd ₅ Si ₂ Ge _{1.9} Fe _{0.1}	<i>c</i>	5	7	276	360
La _{0.8} Ca _{0.2} MnO ₃	<i>c</i>	1.5	5.5	230	66
DyNiAl	<i>c</i>	5	19	256	483
Ni ₂ Mn _{0.75} Cu _{0.25} Ga	<i>c</i>	5	65	308	72
MnFeP _{0.45} As _{0.55}	<i>c</i>	5	18.3	306	390
Fe ₇₀ B ₅ C ₅ Si ₃ Al ₅ Ga ₂ P ₁₀	<i>a</i>	1.5	1.65	~588	74
Fe ₆₀ Cr ₁₄ Cu ₁ Nb ₃ Si ₁₃ B ₉	<i>a</i>	3	0.9	226	38

with a controllable transition temperature over a large range and an excellent MCE can be fabricated; RE-based BMGs that achieve nearly constant $-\Delta S_m$ over a broad temperature range can be obtained. The working-temperature range can be extended to RT with the development of more RE-based BMGs. The devitrification of BMGs is a promising route for preparing nanocrystalline materials that manifest interesting properties. The bulk-glassy alloys and corresponding crystallized composites have the merits of low cost and ease of manufacture without the problem of solid-state reactions between the constituent materials that is usually encountered in multilayered materials.

3.3. Spin Dynamics in BMGs

Spin-glass (SG) materials, including SG-like materials such as surface SG, re-entrant SG, cluster SG and random magnetic systems, bring forward new phenomena and more-complicated problems, and enrich the studies of random and complex systems.^[95–97] Currently, it is unclear whether the inhomogeneous structure from the multiphases can inhibit the critical dynamics and whether multiple SG-like phases can coexist, since most conventional SG materials contain only one SG phase, or coexistence with a ferromagnetic (anti-ferromagnetic) phase. Accordingly, a sample with intrinsic multiple SG transitions is

highly desirable, since it is closely associated with the prototype of multiple complex systems.

3.3.1. Multiple Spin-Glass Behavior in Pr-Based BMGs

The Pr₆₀Al₁₀Ni₁₀Cu₁₆Fe₄ BMG is found to be a model system with intrinsic multiple SG transitions, and this unusual behavior is ascribed to the coupling of the magnetic nanoclusters and the amorphous matrix.^[19] Another factor distinguishing BMGs from conventional SG is the random, single-ion, magnetic-anisotropy interaction which can compete with, or even dominate over the exchange interaction *J*, especially in Nd-, Pr-, Tb-, Ho- and Dy-based BMGs. In SGs, the random-exchange interaction plays the dominant role, and only a slight anisotropy *D* ($\ll J$) exists, but plays a subtle role in the nature of transition.^[95] In the case of a strong RMA limit for $D/J \gg 1$, it is usually described as a speromagnetic (SM) state.^[97] Figure 7 shows the zero-field-cooled (ZFC) and field-cooled (FC) magnetizations of a Pr₆₀Al₁₀Ni₁₀Cu₁₆Fe₄ BMG. A cusp in the ZFC curve and the onset of the irreversibility between the ZFC and FC curves at around 14 K are typical SG features. A careful analysis of the ZFC and FC branches clearly reveals the coexistence of another slight irreversibility between the ZFC and FC curves around $T_{F3} \approx 250$ K, and a sudden increase in the FC magnetization below $T_{F1} \approx 8$ K can also be seen from the inset of Figure 7. It should be noted that the irreversible magnetization near RT is two

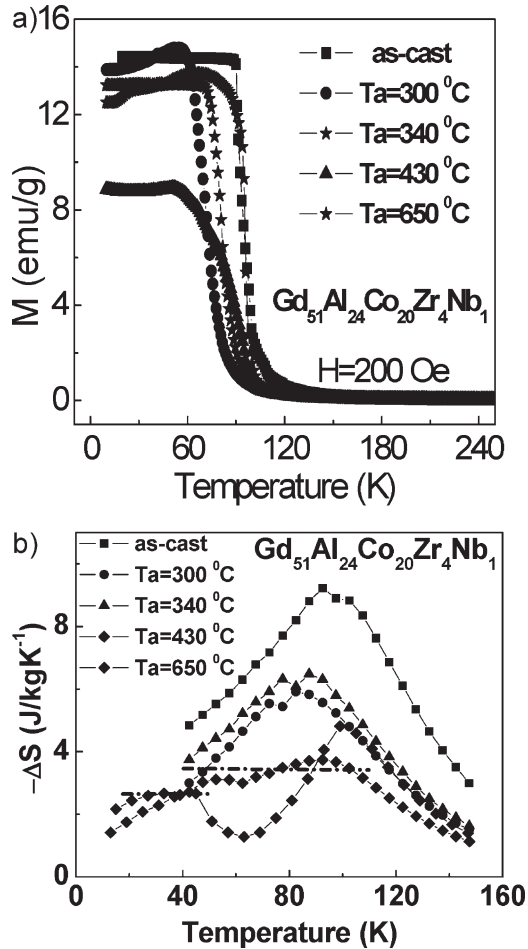


Figure 5. a) Temperature dependence of magnetization under 200 Oe for the as-cast and the annealed $\text{Gd}_{51}\text{Al}_{24}\text{Co}_{20}\text{Zr}_4\text{Nb}_1$ BMGs. b) Magnetic-entropy changes under 5 T. The dashed lines are merely guides for the eyes.

orders of magnitude lower than that around T_{F2} and the peak is rather broad, indicating that some spin clusters are frozen instead of single spin. The coexistence of three different SG phases has also been confirmed through the temperature-dependent ac susceptibility. Figure 8 shows that all of the χ' curves have two maxima, at $T_{F2} \approx 14$ K and $T_{F3} \approx 280$ K, and a small shoulder around $T_{F1} \approx 6$ K, whereas the χ'' curves show three well-defined peaks near T_{F1} , T_{F2} , and T_{F3} . The amplitude and position of all of the peaks or shoulders depend on the frequency. The values of frequency sensitivity at T_{F1} , T_{F2} , and T_{F3} , are determined to be 0.005, 0.012, and 0.01, respectively, falling into the typical range of values for SGs. The frequency dependences of these freezing temperatures are all fitted well by the Vogel–Fulcher formula in Equation (1):

$$\omega = \omega_0 \exp\left(-\frac{E_a}{k_B(T_F - T_0)}\right) \quad (1)$$

The best fitting values are $\omega_{01} \approx 10^{13}$ Hz, $E_{a1} \approx 31$ K and $T_{01} = 4.5$ K; $\omega_{02} \approx 10^{13}$ Hz, $E_{a2} \approx 40$ K and $T_{02} = 12.6$ K; and

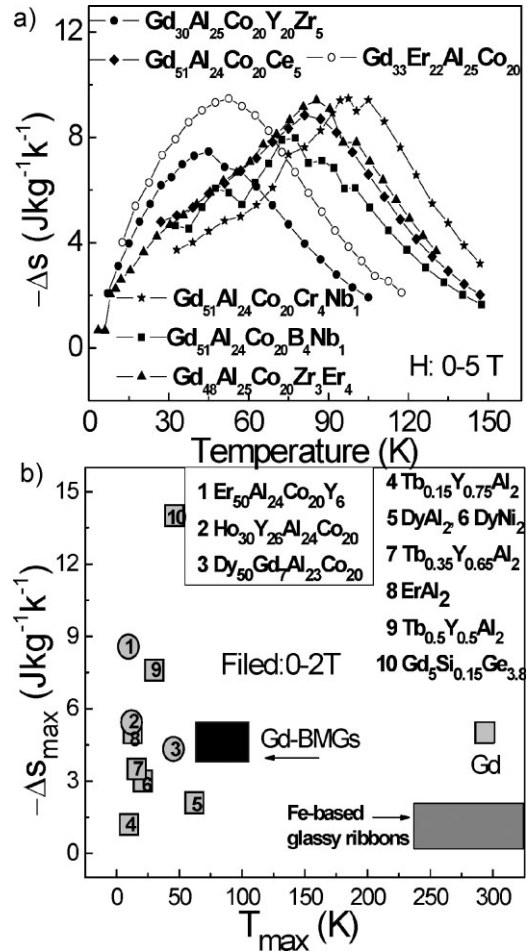


Figure 6. a) Magnetic-entropy changes for six alloying Gd-based BMGs under 5 T. b) Maximal entropy change of various materials under 2 T.

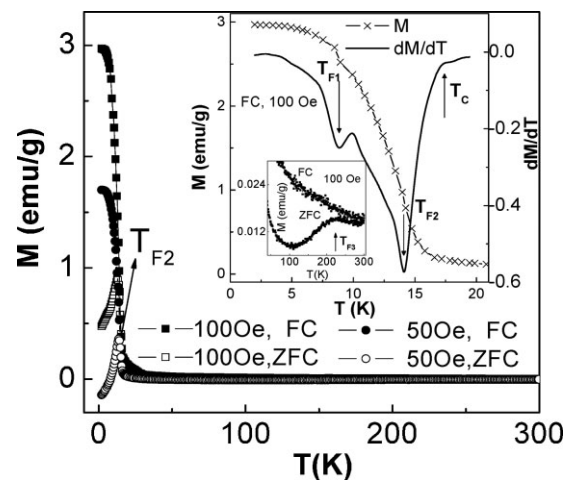


Figure 7. FC and ZFC magnetization measured at 100 Oe and 50 Oe for a Pr-based BMG. The inset shows a typical FC curve: M (left axis) and dM/dT (right axis) measured at 100 Oe. The enlarged FC and ZFC branches at high temperature are also shown in the inset. Reproduced with permission from ref.^[19]; copyright 2007, American Physical Society.

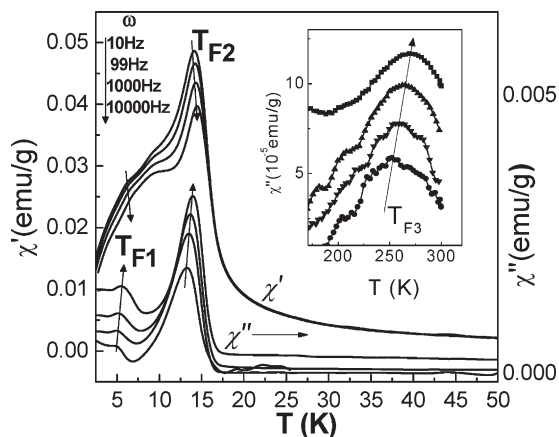


Figure 8. Real (χ') and imaginary (χ'') components of ac susceptibility at frequencies from 10 Hz to 10 kHz under 10 Oe. The inset shows the ac susceptibility at high temperatures. Reproduced with permission from ref.^[19]; copyright 2007, American Physical Society.

$\omega_{03} \approx 10^7$ Hz, $E_{a3} \approx 275$ K and $T_{03} = 233$ K. The value of ω_{03} (10^7 Hz) is much smaller than ω_{01} and ω_{02} (both $\sim 10^{13}$ Hz, just like most SG systems), which suggests that the slower spin dynamics near RT are associated with the relaxation of large spin clusters. The multiple-SG feature is further confirmed by the electric transport property and the glass dynamics.^[19]

Magnetic force microscopy and TEM show some nanoclusters embedded in the amorphous matrix, and the multiple SG behavior is associated with the inhomogeneous microstructure of the Pr-based BMG.^[19] This kind of inhomogeneous nanocluster feature is common for Fe-containing RE-based BMGs. The intrinsic inhomogeneity partially arises from the positive heat of mixing between the Pr (or other RE) and the Fe, which makes the liquid structure less stable and facilitates nanoscale nucleation in the supercooled-liquid state. Accordingly, the cluster-SG freezing at 280 K can be ascribed to the ferromagnetic, Fe-containing nanoclusters. The paramagnetic, Pr-based amorphous matrix and the Pr nanoclusters contribute to the re-entrant SG at $T_{F2} \approx 14$ K, and the cluster SG at $T_{F1} \approx 6$ K. The Pr-based BMGs with different SG phases provide an ideal prototype for a practical understanding of more-complex systems, since most technologically relevant magnetic materials are composed of two (or more) phases with different magnetic properties on the nanometer scale.^[19]

3.3.2. Strong Random Magnetic Anisotropy in RE-Based BMGs

The ground state and the critical dynamics are complicated and obscure due to the disordered structure and the competition between D and J in metallic glasses. These factors have partly been discussed with regard to a $\text{Dy}_{40}\text{Al}_{24}\text{Co}_{20}\text{Y}_{11}\text{Zr}_5$ BMG that exhibits a strong random magnetic anisotropy (RMA).^[36] From the critical and slow dynamics points of view, there are agreements in some aspects between theoretical simulations of Ising spin glasses (ISGs) (and RMA) and experimental results, but also significant quantitative differences exist. For an ISG, an Almeida–Thouless (A–T) line^[98] is theoretically predicted as a

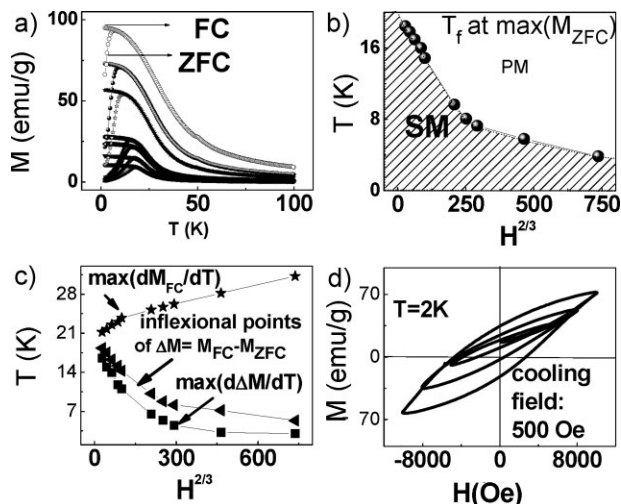


Figure 9. a) Temperature dependence of ZFC and FC magnetization of $\text{Dy}_{40}\text{Al}_{24}\text{Co}_{20}\text{Y}_{11}\text{Zr}_5$. b) Field dependence of T_f . c) Field dependence of other characteristic temperatures. d) Magnetic hysteresis loops between ± 5080 , ± 8080 and ± 10080 Oe at 2 K after field-cooling under 500 Oe. Reproduced with permission from ref.^[36]; Copyright 2008, American Institute of Physics.

transition line in the magnetic field and has been experimentally observed for many SGs. Figure 9 presents ZFC and FC magnetization measurements of the Dy-based BMG; a transition line in the form of an A–T line has been obtained in the low-field regime, suggesting the ISG-like property of the BMG. However, a crossover behavior occurs in the higher-field (above ~ 4000 Oe) region, which may associate with Heisenberg type spin-glass (HSG)-like behavior.^[36] Despite $D \ll J$, the anisotropy can mix the longitudinal and transverse spin components, resulting in only an A–T transition line at the low-field limit like an ISG, and under higher field it recovers its HSG nature. Therefore, the results indicate that some common characteristics exist among real HSG, ISG and strong RMA in the low-field limit. It is found that the susceptibility of 10 Oe superposes on the curve of 0.1 Oe over the whole temperature range, suggesting a linear response to the field perturbation. Similarly, the relationship $\chi''(\omega) = \frac{\pi}{2} \frac{d\chi'(\omega)}{d \ln \omega}$ is precisely obeyed over the whole temperature range, indicating a broad distribution of relaxation times. Furthermore, the relaxation of the low-field ac susceptibility above T_g , reflecting the dynamic spin-correlation function $q(t)$, can be successfully analyzed using an equation similar to the Ogielski function derived from Monte Carlo (MC) simulations on a short-range ISG, which suggests the similarity of RMA and ISGs, especially in the low-field region.

The large random anisotropy has, however, a special impact on the spin dynamics, distinguishing the strong RMA from an ISG in following aspects: firstly, it slows the relaxation of the spins in a critical range near T_g , reflecting the larger characteristic relaxation time, $\sim 10^{-6}$ s, compared with the typical relaxation times of $\sim 10^{-10}$ – 10^{-13} s for SGs. Secondly, it shows slower aging dynamics below T_g and the time-dependent phenomena are well characterized by a power law multiplied by a stretched-exponential functional form, which deviates from the simulation

results of Ogielski and those of some ISGs reported, both showing an algebraic dependence behavior. Thirdly, after cooling in a magnetic field, the spins are in favor of the field direction, and this “frozen” initial magnetization can be “pinned” by the strong RMA, resulting in a vertical shift of the magnetic hysteresis loop in certain fields range. These results indicate that a strong RMA can belong to a different universality class from the (Ising) SG, although several common features are shared between them.

3.4. Heavy-Fermion Behavior of Metallic Glasses

Lanthanides, which are characterized by their narrow 4*f* electronic structure, bring about profuse magnetic and electric properties of RE-based BMGs, such as the superconductivity of La-based BMGs^[55] and the heavy-fermion (HF) behavior of Ce-based BMGs and other BMGs with minor RE element additions. Heavy-fermion systems characterized by electrons with extremely large effective masses have generated considerable interest recently. Many fascinating properties are found in these systems as a consequence of the competition between the local Kondo resonance and magnetic ordering.^[99] It has been recognized that the HF behavior is strongly affected by disorder due to alloying, lattice defects, etc., as manifested by both dynamical mean-field theory and experimental data.^[100–101] What is the nature of the interplay between the degree of disorder in HF materials and their strong-correlation behavior? This remains unclear because only weak disorder exists in intermetallic materials and theoretical models.

In the $\text{Ce}_x\text{La}_{65-x}\text{Al}_{10}\text{Cu}_{20}\text{Co}_5$ BMGs ($x = 0, 10, 20$, and 65 at %), we observe remarkable HF behaviors.^[50] The contribution of the 4*f* electrons to the heat capacity of these alloys is shown in Figure 10a. The linear coefficients γ (C_{el}/T) at 0.53 K for the BMGs with $x = 10, 20$, and 65 are 1789, 2282, and 811 mJ (mol-Ce)⁻¹ K⁻², respectively, indicating the strong HF feature. The change of the low-*T* properties with Ce content is due to the competition between the Kondo effect and the Ruderman–Kittel–Kasuya–Yosida (RKKY) interaction, which is tuned by the average distance between the Ce atoms. Furthermore, it is found that minor Gd alloying (as low as 0.5 at % Gd) can dramatically change the correlations among the electrons in a strongly structurally disordered metallic glass, and tune the CuZrAl (or MgCuY) BMGs with more than 99 at % Cu, Zr and Al to a heavy-fermion alloy with a larger value of the electron specific-heat coefficient.^[56]

The HF behavior can also remain and be tuned by the magnetic field with γ (0 K) reducing to 464 mJ mol-Ce⁻¹ K⁻² at $H = 5 \times 10^4$ Oe for the glass with $x = 10$. The influence of the disordered structure on the competition between the Kondo resonance and magnetic ordering has been studied.^[50] The γ (0 K) decreases with increasing annealing time at temperatures below T_g , inducing the ordering of the structure. This indicates that electric correlations relate closely to the disordered structure of the glass.^[50] In accordance with the theoretic prediction that sufficient disorder can result in a breakdown of the conventional Fermi liquid behavior, these BMGs exhibit non-Fermi liquid features as indicated by the dependence of χ on $T^{-1+\lambda}$ (with

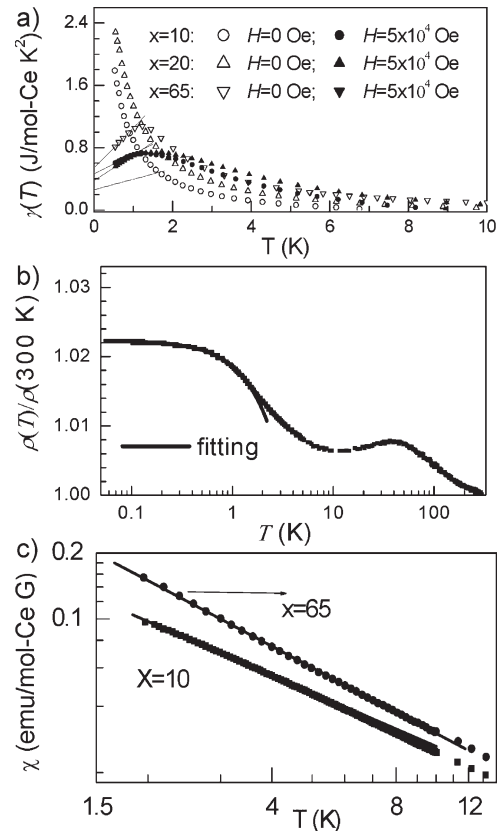


Figure 10. a) $\gamma(T)$ vs. T for $\text{Ce}_x\text{La}_{65-x}\text{Al}_{10}\text{Cu}_{20}\text{Co}_5$ ($x = 0, 10, 20$, and 65) BMGs at $H = 0$ Oe and $H = 5 \times 10^4$ Oe. b) The T -dependent electric resistivity ρ of the BMG ($x = 65$). The solid line denotes the fitting result to $\rho = \rho_0 + AT^n$, with $n = 1.454$. c) The dc magnetic susceptibility χ for $\text{Ce}_x\text{La}_{65-x}\text{Al}_{10}\text{Cu}_{20}\text{Co}_5$ ($x = 10$ and 65) BMGs at low temperature. The solid line is the fitting with $\chi \propto T^{-(1+\lambda)}$. Reproduced with permission from ref. [50: copyright 2007, American Physical Society.

$\lambda = 0.187$ for $x = 10$) and the dependence of the resistivity ρ on T^n ($n = 1.454$) at low temperature (see Fig. 10b–c).^[50,101]

For Ce compounds, when the *f* level of the Ce is right at E_F , strong Kondo resonance overrides the RKKY interaction; when it is far above or below E_F , the local Kondo resonance is weak and the RKKY interaction dominates. It is in the crossover region where the HF behavior happens. Ascribed to the amorphous structure, the distributed *f* levels and the Fermi level within the band of *f* levels of the Ce-based BMGs produce a wide range of strengths of the Kondo resonance and a coexistence of atomic sites in the valence-fluctuation regime, the spin-glass sites dominated by the RKKY interaction, and the crossover sites that show the HF behavior. Accordingly, the reduction of γ by isothermal annealing can be understood by the structural-relaxation-induced narrower *f* levels. The smaller γ for $x = 65$ compared with the other three alloys means that most of the *f* levels sink well below E_F and reduce the HF effect. The heavy-fermion behavior, which can be modulated by the concentration of the minor-alloying atoms, by the degree of spatial disorder and by the magnetic field, is attributed to the structural-disorder-driven hybridization between the conduction

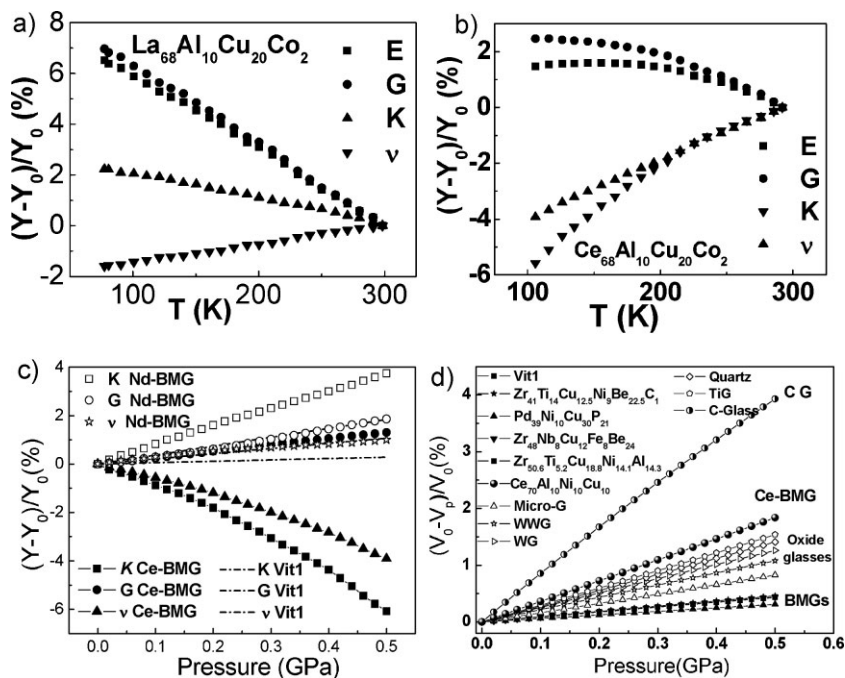


Figure 11. a) Variation of the elastic moduli with temperature for $\text{La}_{68}\text{Al}_{10}\text{Cu}_{20}\text{Co}_2$. b) Variation of the elastic moduli with temperature for $\text{Ce}_{68}\text{Al}_{10}\text{Cu}_{20}\text{Co}_2$. c) Comparison of the relative variations of G , K and ν with pressure up to 0.5 GPa for $\text{Ce}_{70}\text{Al}_{10}\text{Ni}_{10}\text{Cu}_{10}$, $\text{Nd}_{60}\text{Al}_{10}\text{Fe}_{20}\text{Co}_{10}$ and Vit1 at RT. d) The EOS of $\text{Ce}_{70}\text{Al}_{10}\text{Ni}_{10}\text{Cu}_{10}$, other BMGs, oxide glasses and amorphous carbon (CG). The oxide glasses are window glass (WG), water white glass (WWG), fused quartz (Quartz), float glass (NaG) and $\text{SiO}_2 + \text{TiO}_2$ glass (TiG).

and the 4f electrons.^[56] However, revealing the detailed mechanism of the HF of these BMGs remains a challenge.

3.5. Elastic Properties and Possible Polyamorphism in BMGs

The elastic properties and their temperature and pressure dependences provide critical information about the bonding characteristics, microstructure and vibration features of metallic glasses.^[102–119] The temperature dependencies of the elastic moduli for the La- and Ce-based BMGs are shown in Figure 11a–b. With decreasing T , the elastic moduli of $\text{La}_{68}\text{Al}_{10}\text{Cu}_{20}\text{Co}_2$ increase monotonously, indicating the continuous stiffening of the BMG, similar to that of Mg-, Cu-, Zr-based BMGs. For Ce-based BMG, the E and G also display a stiffening mode with decreasing temperature like other BMGs, whereas the K decreases abnormally with decreasing temperature, indicating a remarkable softening behavior. The abnormal behavior of the Ce-based BMG is attributed to the special local structure, especially the alternative valences and unstable electronic configurations of Ce. Since the energy levels of the inner 4f electrons of Ce are so close to those of the outer or valence 5d and 6s levels, only small amounts of energy are necessary to change the relative occupancy of these electronic levels. It has been found that the valence of Ce becomes a non-integral valence, 3.67, below 100 K, in contrast to the value of 3 at RT, corresponding to the lattice collapse arising from the change in electronic structure. Accordingly, the softening of the longitudinal acoustic phonons and the sharp drop of the bulk modulus of the Ce-based BMGs

can be ascribed to the relaxed structure and the shrinkage of the atomic radius owing to the continuously increased valence of Ce upon cooling.^[118]

Experimentally distinguishable responses of the acoustic and elastic properties to pressure, for different kinds of glasses, are observed, which suggests that the short- or intermediate-range ordered local structure determines the elastic and many other properties of various glasses.^[107,112,115,119] Figure 11c presents the pressure dependence of G , K , and the Poisson ratio, ν , for Nd-, Ce- and Zr-based BMGs. For these BMGs the relative change of K with increased pressure is usually larger than that of G and E . The K and ν of the Ce-based BMG exhibit the largest decrease among known BMGs, up to -6.1% and -3.9% at a pressure change of 0.5 GPa, respectively, which reveals a large pressure-induced structural change of the Ce-based BMG. The ν remains nearly constant or shows only slight variations for Nd-, Zr-, Cu-, and Pd-based BMGs, suggesting the unique electric and atomic structure of the Ce-based alloys among the BMG families and the similarity of the structural characteristics between the Ce-based BMGs and the covalently bonded oxide glasses.^[24] It is reasonable to speculate that an amorphous-to-amorphous transition occurs

at higher pressure. Based on the K and its pressure dependence, an isothermal equation of state (EOS) can be established according to the Murnaghan equation.^[120] Typical volume compression of the various glasses is also shown in Figure 11d, from which it can be seen that compressibility of the Ce-based BMG is again closer to that of silicate glasses than that of the other BMGs. Note that the compression curves of the BMGs lie among those of its metallic components and are nearly an average of those of its elements. This is in accordance with the correlation of the elastic moduli of the BMGs with those of their constituents at ambient pressure. Since the compressibility of a solid is determined by the nature of the interatomic potential and the atomic configuration, a good relationship of the compression of BMGs with those of their components implies that the highly packed, short-range-order structure of the BMG has a close relation with the local atomic configurations in their metallic components.

The general consensus is that the best candidates showing polyamorphism are amorphous solids that have directional or open-coordination environments, such as amorphous ice, silica, silicon and chalcogenide glasses.^[121–124] Recently, it has been realized that the preferred bonding characteristic is not necessary for polyamorphism, and polyamorphism has been observed in a Ce-based metallic glass with non-directional metallic-bonding features, different from the network-forming glasses.^[123] The transformation of the low-density glass state to the high-density glass state is ascribed to the interaction of the strongly correlated 4f-electrons and their delocalization under pressure, which results in bond shortening. Our work on the Ce-based BMG has

indicated an anomalous soft behavior both under pressure and under low temperature, similar to that of typical oxide glasses, indeed suggesting a significant structural change (or underlying transformation) under pressure or at low temperature.^[24,118] In a LaCe-based BMG, an unusual change in the compressibility at ~ 14 GPa, suggestive of polyamorphism, is also found.^[124] A possible amorphous-to-amorphous transition has also been suggested in the La- and Nd-based BMGs, from the electrical-resistance behavior under pressure.^[125] The results have implications for the understanding of the microstructure of metallic glasses.

3.6. Polymer-like Thermoplastic Behavior of BMGs – Metallic Plastics

Recently, a series of BMGs with exceptionally low T_g , high thermal stability and a large supercooled-liquid region has been developed.^[12,21,23,43,56,126] These BMGs exhibit the temperature-driven transition from metallic-like to plastic-like behaviors. Figure 12a shows the differential scanning calorimetry (DSC) traces of typical $\text{Ce}_{70}\text{Al}_{10}\text{Cu}_{20}$ and $\text{Ce}_{68}\text{Al}_{10}\text{Cu}_{20}\text{Nb}_2$ BMGs, which are also regarded as metallic plastics.^[12] The T_g of the BMGs is lower than the boiling point of water (100°C) and much lower than that of any other families of BMGs (Fig. 12b), and it is close to that of some amorphous polymers, such as nylon ($\sim 43^\circ\text{C}$), and even lower than that of poly(vinyl chloride) ($75\text{--}150^\circ\text{C}$).^[12,21,23] The stability of these BMGs, in both the supercooled-liquid and the glass states, has been proved by aging experiments.^[12,21,23] For instance, the fully glassy state of Ce-based BMGs is retained even after annealing around its T_g for 147 h, and long-time aging only leads to local structural relaxation but does not have a negative influence on their thermoplastic and mechanical properties. Obviously, stability is necessary for most potential applications.

The most-attractive feature of these BMGs is the temperature-driven metallic-like-to-plastic-like behavior. At RT, and even very close to T_g in the glass state, the alloys are strong and brittle, showing 2% elastic strain followed by catastrophic failure in compression or tension. However, by only raising the temperature to the range near the boiling point of water, the alloys become soft and can be repeatedly compressed, stretched, bent, and formed into complicated shapes as shown in Figure 13. This thermoplastic processing, shaping and forming at such a low temperature range near RT is unusual for conventional metallic materials. Compared with the thermoplastic behavior in the supercooled-liquid states of other BMGs with high T_g , the metallic plastics have remarkable, advantageous properties such as saving energy in manufacturing. Significantly, due to their lack of crystallinity and shrinkage upon solidification, metallic plastics can replicate very-fine microstructures, even on the nanometer scale. This is of great importance for micro-electromechanical systems and other areas where high-precision parts are needed. The precise and smooth patterns demonstrate that the BMGs can be used as potential materials for micro- and nanomanufacturing.^[12,21,23,43,45,56,126] Figure 14 shows the superplastic micro-forming patterns of $\text{Ce}_{70}\text{Al}_{10}\text{Cu}_{20}$ metallic plastic obtained at 420 K in the supercooled-liquid region, which is in the Newtonian

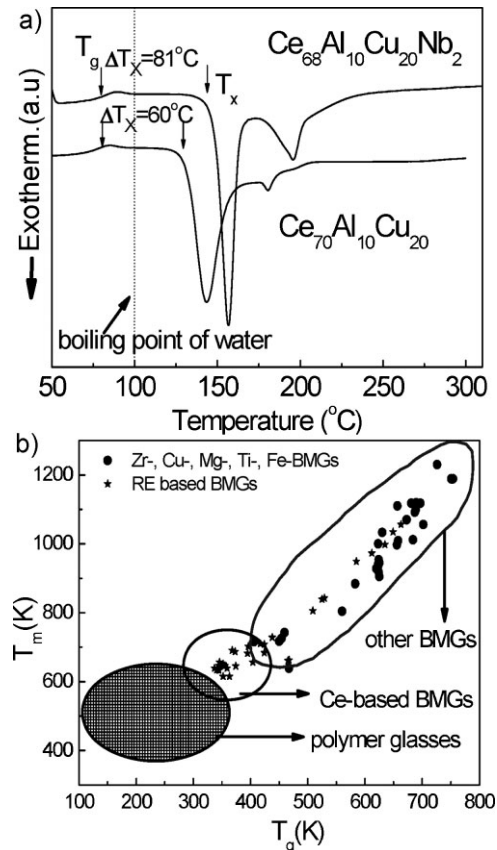


Figure 12. a) DSC traces (10 K min^{-1}) for $\text{Ce}_{70}\text{Al}_{10}\text{Cu}_{20}$ and $\text{Ce}_{68}\text{Al}_{10}\text{Cu}_{20}\text{Nb}_2$ glasses showing the low T_g ($\sim 68^\circ\text{C}$). b) Relation between T_g and T_m for Ce-based metallic plastic, other BMGs and polymer glasses. a) Reproduced with permission from ref.^[12]; copyright 2005, American Physical Society.

flow region, and has the best deformability for the BMG.^[45] The Ce-based BMG fully filled the inside of the Si die. The shapes of the formed samples, with sizes from 3 to $75\ \mu\text{m}$, duplicate the shapes of the Si dies very well. This work demonstrates that the bulk Ce-based metallic glass exhibits superior formability and can be used to fabricate microdevices.

Compared with most polymers, the advantage of metallic plastic is that, when returned to RT after thermoplastic treatment, it resumes metallic-alloy behavior, such as high strength and good electric conductivity. As an example, for $\text{Ce}_{68}\text{Al}_{10}\text{Cu}_{20}\text{Nb}_2$, the density ($6.738\ \text{g m}^{-3}$), elastic modulus, Vickers hardness $\approx 1.50\ \text{GPa}$, fracture toughness $\approx 10.0\ \text{MPam}^{1/2}$, Poisson ratio ≈ 0.32 , and tensile strength $\approx 490\ \text{MPa}$ are all much higher than those of typical polymers. The electrical resistivity of this BMG is $\sim 119\ \mu\Omega\ \text{cm}$, indicating its metallic conductivity, in contrast to the insulating properties of typical polymers. Although cerium metal oxidizes readily, even at RT, the CeAlCu(Nb) BMGs maintain a good surface shine, thus appearing to resist oxidation and corrosion. The high thermal stability with the large supercooled-liquid region provides practical time and temperature scales for heat treatment and thermoplastic processing.^[45] These properties are favored for applications such as micro-machines in nanoimprint lithography, as shown in Figure 13. The demonstration of thermomechanical data storage by forming

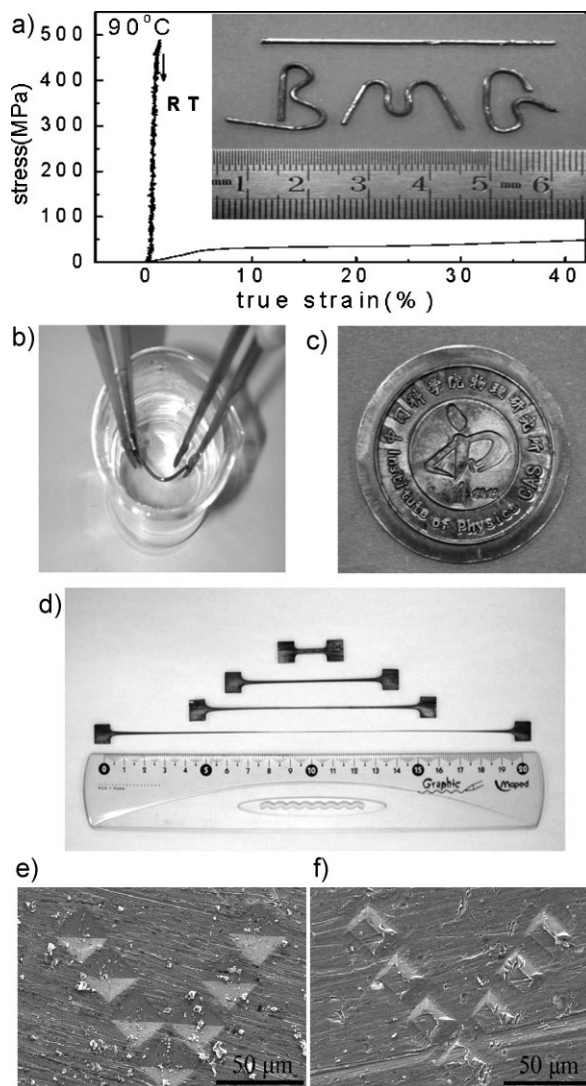


Figure 13. a) True-stress–true-strain curve of a 2 mm diameter $\text{Ce}_{70}\text{Al}_{10}\text{Cu}_{20}$ glassy rod tested under compression at RT and at 90°C . The inset shows the glassy rods formed into letters by simple manipulation in near-boiling water as shown in b). c) Impression of the badge of the Institute of Physics of the Chinese Academy of Sciences made while held in near-boiling water, demonstrating excellent imprintability and viscous deformability. d) The initial and elongated samples of the $\text{Ce}_{69}\text{Al}_{10}\text{Cu}_{20}\text{Co}_1$ metallic plastic. e) A ‘V’ pattern shaped by a Vickers hardness tester on the surface of the mold. f) The successfully replicated ‘V’ pattern on the surface of the BMG sheet held in hot silicon oil, exhibiting excellent imprintability and viscous deformability. Images (a,b) reproduced with permission from [12]. Copyright 2005, American Physical Society. Images (e,f) reproduced with permission from [126]. Copyright 2008, American Institute of Physics.

nanoindentations through Joule heating of scanned nanotips uses a polymer as the storage medium.^[127] The writing and erasing processes suggest that the BMGs may offer a viable alternative for rewritable, high-density data-storage technology. For this application and for imprintability, there is an advantage in the increased precision when the medium has higher elastic moduli. The metallic plastics have Young’s moduli many times those of typical polymers, while their low T_g means that no-more energy is needed than for polymer imprinting. The electrical

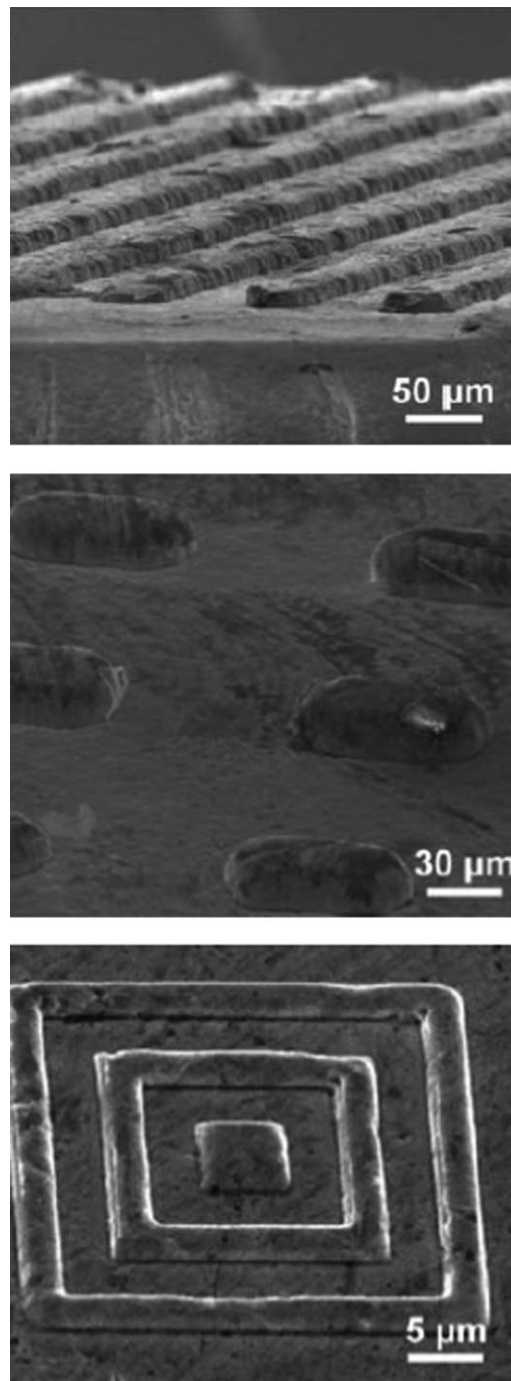


Figure 14. SEM images of various patterns obtained by microforming $\text{Ce}_{70}\text{Al}_{10}\text{Cu}_{20}$ metallic plastic at 420 K. Reproduced with permission from Ref [45], copyright 2006, Elsevier.

resistivity of the metallic plastics indicates that this alloy is a metallic conductor, in contrast to the insulating properties of typical polymers. It may also be useful for this imprintability to be combined with electrical conductivity. Note that, by using the elastic-modulus rule for smart selection of components with suitable elastic moduli, more polymer-like BMGs with excellent thermoplastic properties for such promising applications as

high-performance microstructures and micromachines can be developed.

BMGs with low T_g can be used as both the mold and the materials from which nanostructures and microstructures are formed or imprinted. A familiar challenge is to find a low-cost, durable means of molding features on the nanoscale into materials currently used in the manufacture of devices such as computer chips. Nano- and microscale imprinting would replace the lithographic technique currently used to make computer chips. Metallic plastics are expected to open up much-broader applications in the near future.^[12,21,23,43,56,126]

3.7. Excellent Wave-Absorption Ability of BMG Composites containing Carbon Nanotubes

The mechanical properties of BMG composites can be significantly improved when the material is reinforced with metals or metal fibers,^[128] and unique properties can be introduced into BMG composites by adding some crystalline functional materials. Carbon nanotubes (C nanotubes), as the “ultimate” carbon fiber with special functional properties,^[129] can also be introduced into a BMG matrix, and lead to unique mechanical and special functional properties, such as excellent wave-absorption ability.^[111] Figure 15 shows a typical TEM morphology of C nanotubes distributed in a Zr-based BMG matrix. The tubular shape and the whole carbon nanotubes are clearly observed in the glassy matrix, as shown in Figure 15a–b. The C nanotubes only partially react with the glass matrix and most of them still keep their tubular and multiwalled structure. This means that the added C nanotubes basically keep their primary structure, implying that they can also keep their excellent mechanical or functional properties. The BMG composites, which are the mixed structure of the residual C nanotubes and the ZrC phase, disperse randomly in the glassy matrix, and have significantly better mechanical properties than the unenhanced BMGs.^[111]

The remarkable result is that the addition of C nanotubes causes significant acoustic-wave attenuation in the BMG (shown in Fig. 15c). The values of α_l (longitudinal wave-attenuation coefficient) and α_t (shear wave-attenuation coefficient) increase notably with a tiny increase in the amount of C nanotubes added. For adding 4 vol % C nanotubes, α_l is 10 times larger and α_t nearly 7 times larger than those of the undoped BMG. Even an addition of 1 vol % causes very-large relative changes in α_l and α_t (440% and 255%, respectively). The values of the acoustic velocities could not be obtained for more C-nanotubes addition because the ultrasonic attenuation was so strong that no pulse echo could be observed under experimental conditions. The above results imply that the addition of C nanotubes into the Zr-based BMG matrix causes strong wave absorption.^[111] The excellent wave-absorption ability of the composites originates from the random dispersion of the residual C nanotubes and the ZrC phase (induced by the interfacial reaction between the glassy matrix and the added C nanotubes), the formation of new interfaces, and the denser packed structure in the glass matrix of the composites. The composites could have potential application in isolating acoustic sound or blocking out environmental noise.

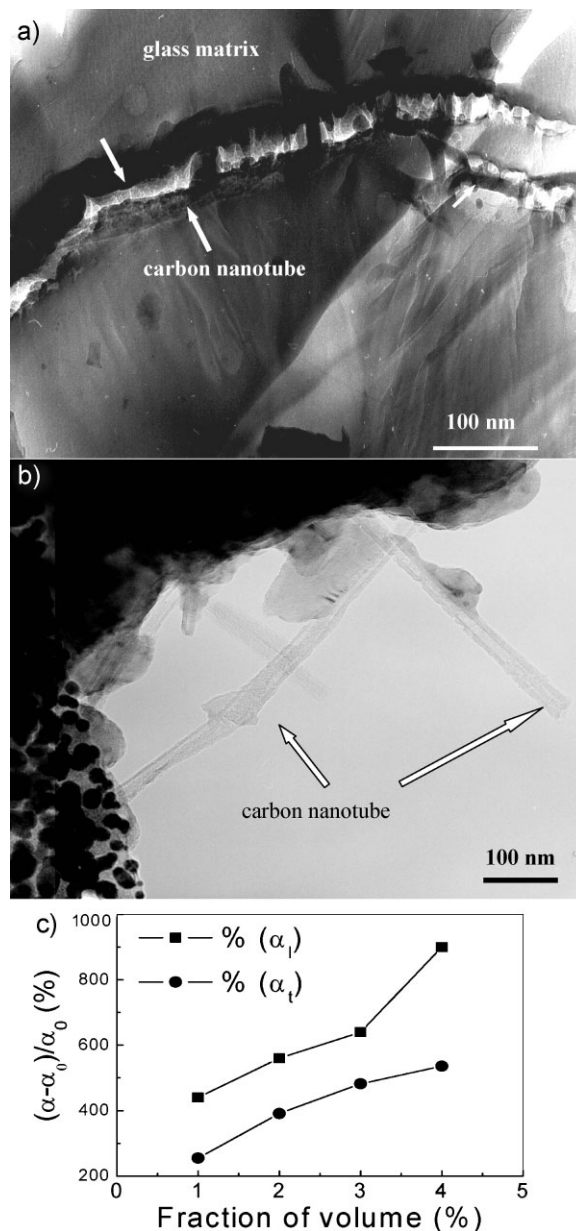


Figure 15. a)–b) Carbon nanotubes distributed in Zr-based BMG matrix. c) Relative changes, $\Delta\alpha/\alpha_0 = (\alpha - \alpha_0)/\alpha_0$ of the variation of the longitudinal and transverse ultrasonic attenuation (α_l and α_t) of Zr-based BMG composites, on increasing the volume fractions of carbon-nanotube addition. (α_0 is attenuation coefficient of the undoped BMG; α is the attenuation coefficient of composites). Reproduced from [111].

3.8. Spontaneous Formation of Nanostructures by Fracture of BMGs

One of the most-active trends in material science is the development of synthetic methods to obtain shape- and size-controlled nanostructures, since the physical and chemical properties of nanostructures are strikingly sensitive to both morphology and size.^[130–131] The categories of metallic alloys and metal oxide nanostructures are important and have been

extensively studied due to their scientific interest and practical applications. However, while research has demonstrated the superiority of the amorphous state over the crystalline state for most applications, it has been found that most of these metallic nanostructures are crystalline.^[132] Recently, it has been predicted theoretically and confirmed experimentally that the amorphous state is naturally favorable for stable nanostructures, making them more feasible.^[133–134] In BMGs, the plastic deformation at room temperature is highly localized in nanoscale shear bands, where a large plastic strain is accumulated in a very-thin region (10–20 nm thick), exhibiting strain softening or thermal softening.^[135] The softening leads to the formation of a viscous, fluid-like layer which manifests itself in remarkable patterns when the shear band comes apart in the final fracture. Using the unique nature of the localized plasticity, the spontaneous formation of metallic-glassy nanostructures can be realized by simply fracturing the BMGs at room temperature.^[136] Because of the original metallic-glass state and the extremely high cooling rate in the plastic zone at the crack tip during fracture, the nanostructures so formed are also in the glassy state. The fracture was performed by conventional three-point-bend testing with a constant displacement velocity of 0.5 mm min⁻¹ at room temperature. The fracture surface observed by scanning electron microscopy (SEM) is predominantly characterized by a typical vein pattern on the relatively smooth crack plane.^[67] With further observations by high-resolution SEM, one can find various morphologies of nanostructures on the fracture surfaces of BMGs. Figure 16a clearly shows a portion of a nanoridge with an approximately triangular cross section, ~250 nm wide at the base and ~350 nm high, in a fracture surface of a Ce-based BMG. When the nanoridges meet, a nanocone can be readily found in the vicinity of the intersection (Fig. 16b). A uniform nanowire ~340 nm in diameter and ~19.6 μm in length can also be seen, formed from similar intersections and attached to the fracture surface, as shown in Figure 16c. Many spheres ranging from tens to hundreds of nanometers in diameter can again be found, as shown in Figure 16d. Nanoscale, striped patterns with a spacing of ~70 nm have been observed on fracture surfaces in other brittle BMGs (Fig. 16e–f).^[67]

In standard fracture mechanics it is accepted that there is a well-defined plastic zone at the crack tip. The plastic-zone size, l_p , of BMGs for crack propagation under plane strain can be expressed approximately as:^[67,137]

$$l_p = 0.025(K_C/\sigma_y)^2 \quad (2)$$

In Equation (2), K_C is the fracture toughness and σ_y is the yield stress. The typical vein size, w , and l_p for a very-broad range of BMGs have been confirmed experimentally to scale with $w \approx l_p$.^[67] The maximum temperature rise in the narrow plastic zone of the Ce-BMG is estimated to be ~1000 K, which fits with experimental observations on shear bands.^[138] High temperatures in the plastic zone rapidly decrease through heat conduction to the surrounding bulk, and the cooling rate is estimated to be $\sim 2 \times 10^6 \text{ K s}^{-1}$.^[138] The cooling rate greatly exceeds the critical cooling rate for glass formation (10^2 K s^{-1} for the Ce-based BMG^[20]), and ensures the glassy nanostructure.

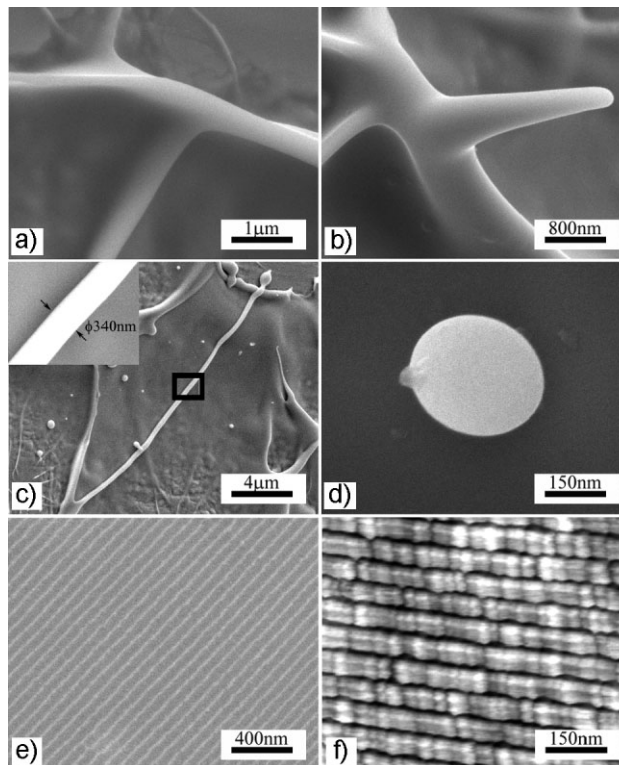


Figure 16. a)–d) Fine nanostructures on the fracture surface of Ce-based BMG. a) A portion of a nanoridge constituting the typical vein pattern. b) A nanocone in the vicinity of a ridge intersection. c) A uniform nanowire with a diameter of 340 nm. d) A nanosphere with a diameter of 180 nm. e) SEM image of a nanoscale, striped pattern with a spacing of ~70 nm on the fracture surface of a Mg-based BMG. f) Atomic-force-microscopy (AFM) image of a nanoscale, striped pattern with a spacing of ~70 nm on the fracture surface of a Mg-based BMG. a)–f) Reproduced with permission from [136]. Copyright 2009, Materials Research Society.

The nanoscale plastic zone offers a natural “laboratory” for studying the formation of metallic nanostructures. As the crack advances into the plastic zone with much-reduced viscosity, a viscous fingering pattern appears at the crack tip due to the meniscus instability. The finger walls act as discontinuous viscous bridges and undergo plastic deformation via a one-dimensional necking process under tensile stress, leading to tapered nanoridges, wide at the base and sharp at the top. If these nanoridges meet, the situation is more complicated and a cylindrical liquid bridge emerges (Fig. 16b). Plastic deformation of a cylindrical liquid-like bridge under tension can lead to necking (Fig. 16c) and the formation of two well-aligned nanocones. Alternatively, with suitable local viscosity and strain rate, the cylindrical liquid-like bridge behaves in a superplastic manner and can be stretched uniformly thousands of percent without necking (Fig. 16d). Additionally, if the local viscosity is too low or the local strain rate too high, the deformation and final rupture of the viscous materials in the plastic zone break up the viscous bridges and, through a Rayleigh instability, can give rise to some individual spheres.

These length scales of the nanostructures on the fracture surfaces of BMGs have been found to correlate with the mechanical properties.^[136] Figure 17a–d shows characteristic

nanospheres on fracture surfaces for a variety of BMGs. The sizes of the nanospheres are very different for different BMG systems. Figure 17e and 17f show the clear relationship between the average largest-sphere diameter, D , the average width of the nanoridges, W , and the vein size, w , and the relevant values are given in Table 3. Intrinsically, the l_p of the BMGs ranges broadly from ~ 1 mm for tough Zr-based BMGs down to ~ 10 nm for brittle Fe-based BMGs.^[67] The D - and W -curves have a similar shape and the values generally increase with increasing w . The links of the dimensions of the nanostructures (i.e., D and W) to w indicate that w can be determined from the fracture toughness and yield stress of a BMG.^[136] The clear correlation between the mechanical behavior of BMGs (K_{IC} , σ_y and Poisson's ratio ν) and the nanostructural dimensions assists in approximately controlling the size of the nanostructures spontaneously formed by fracture of appropriate BMG systems by varying the size of the plastic zone. The plastic-zone size can also be tuned by gradually changing the mechanical properties of the BMGs through extrinsic methods such as annealing,^[15,64,67] and can in turn control the size of the nanostructures. The reported, spontaneous formation of various nanoscale structures with a tunable size in metallic glass simply by fracturing a metallic glass offers an easy technique for the fabrication of amorphous, metallic, nanoscale structures with high strength and high corrosion resistance, which might be applicable and provide building blocks for the development of small devices. The spontaneous formation of nanoscale-metallic-glass striped patterns has application potential such as in nanoscale gratings or ultraminiaturized integrated circuits.

3.9. Multifunctional CaLi-Based Bulk Metallic Glasses

A new class of CaLi-based BMGs consisting of cheap main components, Ca, Mg and Li, simultaneously offering excellent GFA and unique properties has been reported.^[126,139] As contrasted in Figure 18, the T_g of the CaLi-based BMGs approaches RT, and the lowest value is $\sim 35^\circ\text{C}$ for $\text{Ca}_{65}\text{Li}_{14.54}\text{Mg}_{12.46}\text{Zn}_8$. These BMGs have, to date, the lowest T_g of known metallic glasses. The results show that it is possible to get BMGs with low T_g close to RT: these are more likely to exhibit ductility and even superplasticity at room temperature. The larger supercooled-liquid temperature region, ΔT , indicates a high thermodynamic stability of their supercooled-liquid state.^[1-6] The BMGs have much-greater kinetic stability than other low- T_g metallic glasses when aged below T_g , which is also testified by a temperature–time–transition (TTT) diagram.^[126] The crystallization-incubation time around T_g is about 1 h. The exceptionally low T_g and remarkable stability of the supercooled-liquid state of the glass provides great convenience for formability and manufacturability.^[126] At around 50°C , the alloys can be repeatedly compressed, stretched, bent, and formed into complicated shapes.

The density, Vickers hardness H_v , E , K , G , ν and fracture strength σ of typical $\text{Ca}_{65}\text{Li}_{9.96}\text{Mg}_{8.54}\text{Zn}_{16.5}$ glass are determined to be 1.956 g cm^{-3} , 1.35 GPa , 23.4 GPa , 20.2 GPa , 8.95 GPa , 0.307 , and 530 MPa , respectively. Due to the ultralow density, the glass exhibits a specific strength (σ/ρ) of $271\text{ MPa} \cdot \text{cm}^3 \cdot \text{g}^{-1}$, which is

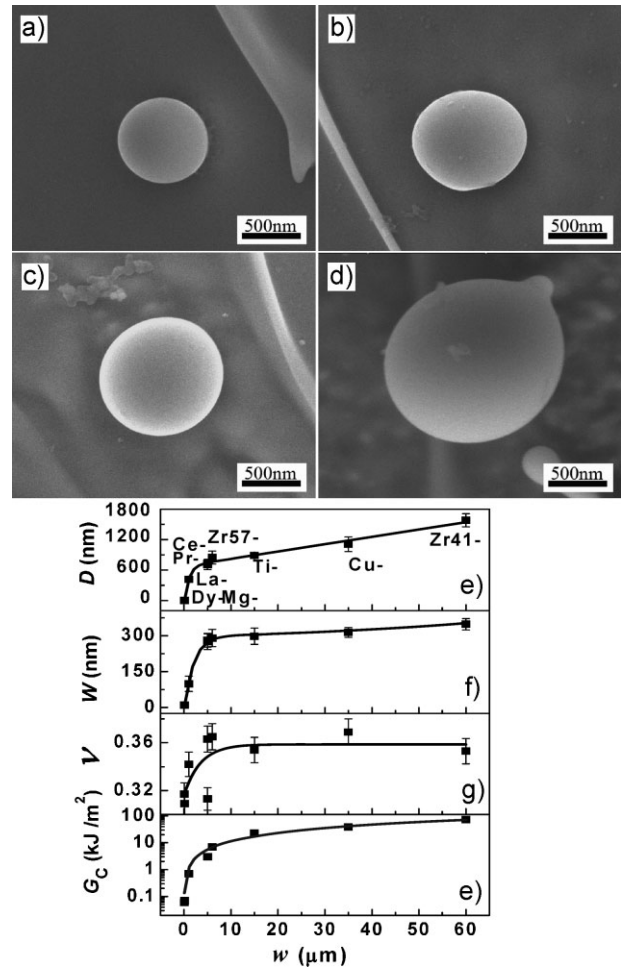


Figure 17. a) SEM image of the characteristic largest nanospheres for a Ce-based BMG. b) SEM image of the characteristic largest nanospheres for a $\text{Zr}_{57}\text{Cu}_{15.4}\text{Ni}_{12.6}\text{Al}_{10}\text{Nb}_5$ BMG. c) SEM image of the characteristic largest nanospheres for a Cu-based BMG. d) SEM image of the characteristic largest nanospheres for a $\text{Zr}_{41.2}\text{Ti}_{13.8}\text{Cu}_{12.5}\text{Ni}_{10}\text{Be}_{22.5}$ BMG. In a)–d), the BMGs were fractured under the same conditions. e) Dependence of the average diameter of the largest spheres D on the typical vein size w on the same fracture surface for a range of BMGs. f) Dependence of the width of nanoridges W on the typical vein size w on the same fracture surface for a range of BMGs. g) Dependence of Poisson's ratio ν on the typical vein size w on the same fracture surface for a range of BMGs. h) Dependence of the fracture energy G_{IC} on the typical vein size w on the same fracture surface for a range of BMGs. a)–h) Reproduced with permission from ref.^[136]; copyright 2009, Materials Research Society.

about the same magnitude as that of Zr-based BMGs^[2-6] and about 40% higher than that of conventional crystalline Mg-alloys. Figure 18 also shows the comparisons of E and ρ between $\text{Ca}_{65}\text{Li}_{9.96}\text{Mg}_{8.54}\text{Zn}_{16.5}$ and other BMGs.^[126] It shows clearly that the E of the BMG is the lowest in all known BMGs. The combination of desirable properties in the CaLi-based BMGs is attributed to the fact that Li has the lowest E (4.9 GPa) and ρ (0.525 g cm^{-3}) of the metal elements, according to elastic-moduli correlations.^[15] The Li content can effectively modulate the properties of CaLi-BMGs, and the T_g decreases monotonically with the increase of the content of Li. Other properties of the BMGs can also be controlled by Li content.

Table 3. The parameters of vein size (w), the average diameter of the largest spheres (D), width of nanoridge (W), elastic-modulus ratio (G/K), Poisson ratio (ν) and fracture energy (G_c) of a range of typical BMGs.^[136]

BMGs	w [μm]	D [nm]	W [nm]	G/K	ν	G_c [kJ m^{-2}]
Dy ₄₀ Y ₁₆ Al ₂₄ Co ₂₀	0.08	–	10	0.417	0.317	0.06
Mg ₆₅ Cu ₂₅ Tb ₁₀	0.1	–	10	0.439	0.309	0.07
La ₅₅ Al ₂₅ Cu ₁₀ Ni ₅ Co ₅	1	417 ± 39	99 ± 32	0.354	0.342	0.7
Pr ₆₀ Al ₁₀ Ni ₁₀ Cu ₂₀	5	709 ± 100	281 ± 29	0.302	0.363	–
Ce ₇₀ Al ₁₀ Cu ₁₀ Ni ₁₀	5	731 ± 60	275 ± 33	0.427	0.313	3
Zr ₅₇ Cu _{15.4} Ni _{12.6} Al ₁₀ Nb ₅	6	848 ± 127	290 ± 36	0.297	0.365	7
Ti ₄₀ Zr ₂₅ Ni ₃ Cu ₁₂ Be ₂₀	15	886 ± 58	298 ± 34	0.324	0.354	22.74
Cu ₆₀ Zr ₂₀ Hf ₁₀ Ti ₁₀	35	1110 ± 145	314 ± 21	0.288	0.369	38
Zr _{41.2} Ti _{13.8} Cu _{12.5} Ni ₁₀ Be _{22.5}	60	1583 ± 128	348 ± 24	0.324	0.353	72

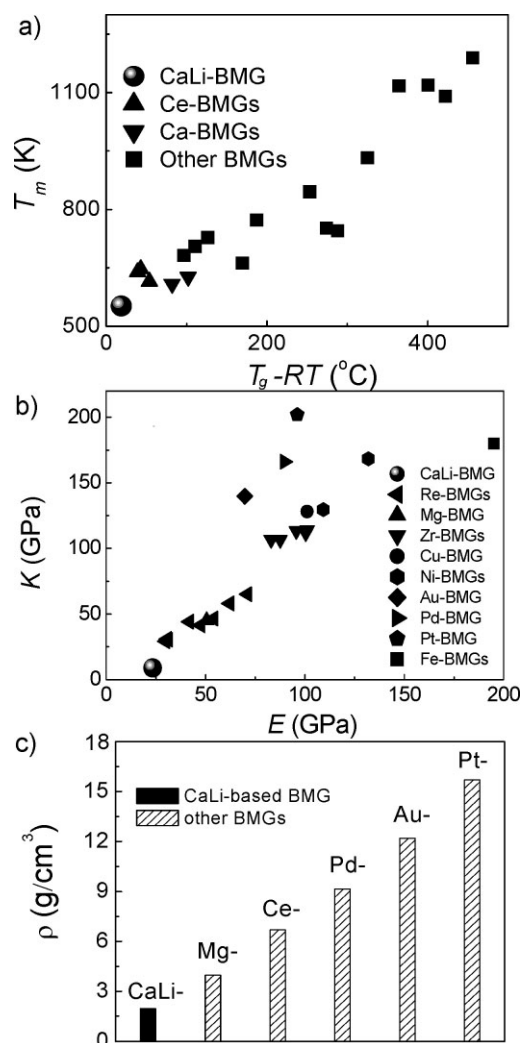


Figure 18. a) Comparison of T_g and melting temperature T_m for Ca₆₅Li_{9.96}Mg_{8.54}Zn_{16.5} with other BMGs. b) Comparison of E for Ca₆₅Li_{9.96}Mg_{8.54}Zn_{16.5} with other BMGs (RE-BMG stands for rare-earth-based BMGs). c) Comparison of ρ for Ca₆₅Li_{9.96}Mg_{8.54}Zn_{16.5} with other typical BMGs (Mg-, Ce-, Pd-, Au- and Pt-based BMGs) with T_g lower than 600 K. a)–c) Reproduced with permission from ref.^[126]: copyright 2008, American Physical Society.

Multifunctional BMGs with the lowest T_g , exceptional thermodynamic and kinetic stability, ultralow elastic moduli and density, ultrahigh specific strength and elasticity, very-low electrical resistivity, and unusual mixture of near-ambient-temperature plasticity and metallic properties could have potential in various applications. For example, artificial bone must have enough strength and an appropriate E that is comparable with that of human cortical bone (2–18 GPa) to decrease the mechanical inelasticity between the implanted bone and human bone. Ti alloys (e.g., Ti-6Al-4V), as a common, bone-implant material, however, have larger ρ and E than that of natural human bone. This is considered to be a distinct disadvantage because it may cause a mechanical incompatibility. Ca is a bioelement and CaLi-based BMGs combining low ρ , high strength and an E that is comparable to human bone might have potential applications as biomaterials. Although the alloys containing Ca and Li are highly susceptible to corrosion and oxidation and Li is generally considered to be toxic for in vivo applications, an appropriate surface process such as coating may be effective in minimizing these negative effects. The main components of the BMGs are the strong hydrogen-getters of Ca, Mg and Li; these elements show excellent affinities for hydrogen and form hydrides, MgH₂, CaH₂ and LiH.^[140] CaLi-based BMGs, with low density and low cost, potentially present hydrogenation and hydrogen desorption at a low temperature owing to the low temperatures of T_g and T_x , which may indicate that the glasses are potentially good hydrogen-storage materials.

The surface of traditional glasses obviously plays an important role in the performance of the entire system in practical applications, while little attention has been paid to the surface of BMGs. Wettability is an important property of a solid surface and plays an important role in daily life, industry, and agriculture, as well as in biological processes, such as in the prevention of the adhesion of snow to antennas and windows, self-cleaning traffic indicators, the reduction of frictional drag on ship hulls, metal refining, stain-resistant textiles, and cell motility.^[141] In nature, lotus surfaces, with simple epicuticular wax and a special surface morphology, are superhydrophobic. Dirty particles can be removed by water droplets that roll off the surfaces, independent of their chemical nature or size. This is called the lotus effect.^[142] A simple and feasible method for the construction of stable superhydrophobic and superoleophobic surfaces can be realized

using BMGs based on active elements such as Mg, Ca, or rare-earth elements with poor corrosion resistance.^[15] The synthesis strategy consists of fabrication of micro- and nanoscale hierarchical surface structures and the modification of surfaces using thin films with low surface energy, such that the obtained BMG surface has a dramatically improved corrosion resistance and highly stable superamphiphobicity.^[139] For example, to prepare the superhydrophobic surface of a $\text{Ca}_{65}\text{Li}_{10}\text{Mg}_{8.5}\text{Zn}_{16.5}$ BMG, the BMG sheets were first soaked in doubly distilled water for several minutes. The BMGs was etched by water owing to its water-dissolving feature. Then, the sample surface was modified with a 1.0% ethanol solution of fluoroalkylsilane (FAS) for 12 h: the surface of the BMG was fully covered by the FAS film, which served as a barrier against a hostile environment. The as-cast CaLi-based BMGs are highly susceptible to corrosion of water and other chemical matters and oxidation. The modified BMG can be kept safely under ambient conditions for long time. The FAS film with low surface energy can also lead to hydrophobic or oleophobic surfaces.

SEM images of the BMG surfaces before and after treatment are shown in Figure 19. Before treatment, the BMG surface is flat with only a few impurities (smaller than $1\ \mu\text{m}$) scattered on it (Fig. 19a and 19b). After treatment, the BMG surface shows a coral-like pattern on the micrometer scale (Fig. 19c–d), and small protrusions aggregate on the micrometer-level configurations with some rod-like outshoots on top of each protrusion. The average size of a protrusion is about $100\ \text{nm}$. The treated BMG surface actually has microscale–nanoscale hierarchical structures, which dramatically increase the surface roughness. The shape of a water droplet on the untreated BMG surface is shown in Figure 20a, which demonstrates the hydrophilic property of the untreated BMG sample. Figure 20b–c presents a water droplet and an oil droplet on the BMG surfaces modified with FAS, respectively, where each droplet is in a perfectly spherical shape riding on top of the surface, indicating the superhydrophobic and superoleophobic properties. The water and oil contact angles, θ ,

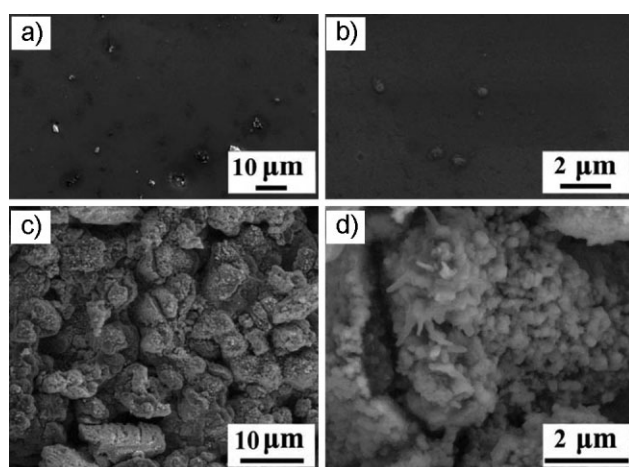


Figure 19. SEM images of aCaLi-based BMG's surfaces. a) Low-magnification SEM image of the surface before treatment. b) HR-SEM image of the surface before treatment. c) Low-magnification SEM image of the surface after treatment. d) HR-SEM image of the surface after treatment. a)–c) Reproduced with permission from ref.^[139]: copyright 2009, Elsevier.

are $162 \pm 2^\circ$ and $156 \pm 3^\circ$, respectively. Furthermore, the water droplets are hardly able to stick to the modified BMG surfaces, and roll off quite easily, which demonstrates the self-cleaning effect and resembles the lotus effect. Figure 20d shows a photograph of a water droplet (about 7 mg) sitting on the treated BMG surface after the sample had been exposed to air for more than three months. The spherical water droplet is located on the treated BMG surface, which indicates the resultant BMG surface modified with FAS possesses a stable superhydrophobic property and good corrosion resistance. The wettability of the solid surfaces is influenced by both the surface morphology (surface roughness) and the chemical composition.^[143] The presence of the binary microscale–nanoscale hierarchical structures dramatically increases the surface roughness of the BMG surface, which greatly minimizes the contact area between the water droplets

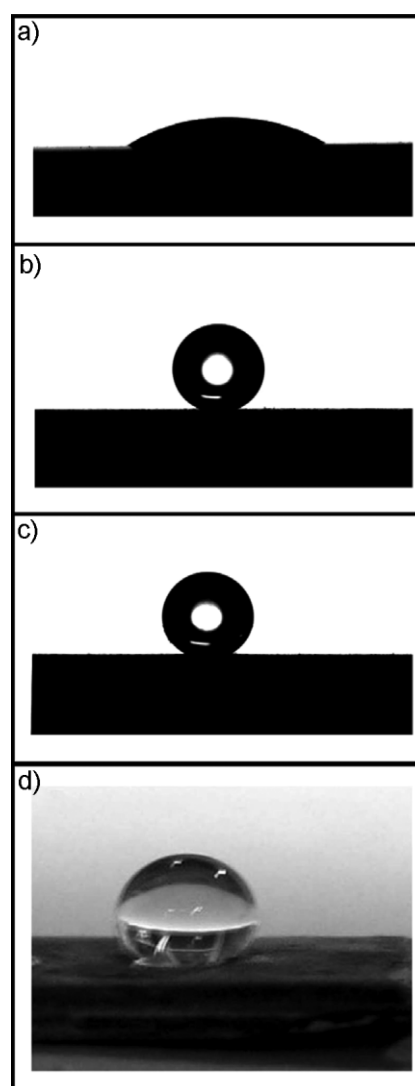


Figure 20. Droplet shapes on the surface of CaLi-based BMGs. a) Water-droplet shape on the untreated BMG surface. b) Water-droplet shape on the treated BMG surface. c) Oil-droplet shape on the treated BMG surface. d) Photo image of water droplet on the treated BMG surface after the surface was exposed to air for three months. a)–d) Reproduced with permission from ref.^[139]: copyright 2009, Elsevier.

and the BMG surface. On the other hand, a large θ value is achieved via the low surface energy of the FAS coating. Together, the microscale–nanoscale hierarchical structures and the FAS coating result in stable superhydrophobic and superoleophobic states.

4. Summary and Outlook

As a frontier of metal research, metallic glasses have attracted intense research interest in recent decades and are now among the most-actively studied metallic materials, and the bulk-metallic-glasses field is progressing fast. A series of BMGs have been developed and much attention has been paid to the mechanical properties of the novel materials because BMGs are regarded as possible, ideal, future, engineering materials. However, some unresolved issues such as limited glass-forming ability, brittleness, cost and process difficulties restrict the applications. This paper focuses on a variety of bulk metallic glasses that could have potential applications as functional glassy materials. These metallic glasses, with excellent glass-forming ability, have been found to display many fascinating properties, such as excellent wave-absorption ability, exceptionally low glass-transition temperatures approaching room temperature, ultralow elastic moduli comparable to that of human bones, high elasticity (2%) and high strength, superplasticity and polymer-like thermoplastic formability near room temperature, excellent magnetocaloric effect, hard magnetism and tunable magnetic properties, heavy-fermion behavior, superhydrophobicity and superoleophobicity, polyamorphism, and so on. Concerning the design of new metallic glassy compositions, the “elastic-modulus rule”^[15] can guide one to search and effectively develop BMGs with good glass-forming ability and unique functional properties, or controlled/desired properties based on the elastic moduli.

With the development of more novel BMG systems and their derivatives, it is expected that more unique mechanical, physical and chemical properties of BMGs will be explored, and the main commercial prospects of BMGs lie in their high performance in applications as functional materials. Broader usage as magnetic-recording/storage materials, micro-electromechanical systems, nano- and microdevices, high-density rewritable devices, hard magnets, magnetic refrigerants and magnetostriction materials can be expected in the future. Applications of BMGs as functional materials can avoid the intrinsic flaws of BMGs and broaden their application field. Another advantage for applications of these BMGs as functional materials is that there are more degrees of freedom to tailor the electric, mechanical and magnetic properties owing to the flexibility in composition, microstructural manipulation, shape and dimensions of the new glasses. Furthermore, the polymer-like thermoplasticity in the supercooled-liquid-temperature region of the BMGs enables their products to be obtained in a one-step process in different shapes (such as spheres, balls, thin sheets or plates, wires, rings, rods and others). All of these would permit more-widespread, cost-effective applications of the novel BMG materials, in comparison to the earlier stage of the development of metallic glasses.

BMGs with functional physical properties are of interest, not only for their technological applications, but also for basic research. For the fundamental aspects, the BMGs, which exhibit profuse and versatile physical properties and phenomena, such as

low-temperature thermoplasticity, spin-freezing dynamics, hard magnetism, heavy-fermion behavior and polyamorphism, open up more challenges and opportunities for glass sciences. These metallic glasses are a particularly good testing ground for condensed-matter theories.^[144–148]

Therefore, the development and study of BMGs with functional physical properties will reward more attention. The synergies between engineering and functional explorations and between fundamental and applied studies should make BMGs significant materials in the future.

Acknowledgements

This work receives ongoing support from the Natural Science Foundation of China (Nos. 50731008 and 50621061), the national fund for fundamental key projects MOST 973 (No. 2007CB613904) and the Chinese Academy of Sciences. We are grateful for the contributions to the work by all of the group members. This paper is part of a Special Issue on research at the Institute of Physics, Chinese Academy of Sciences.

Received: March 27, 2009

Published online: September 15, 2009

- [1] a) A. MacFarlane, G. Martin, *Science* **2004**, *305*, 1407. b) P. W. Anderson, *Science* **1995**, *267*, 1615.
- [2] J. J. Gilman, *Science* **1980**, *208*, 856.
- [3] a) B. X. Liu, W. S. Lai, Q. Zhang, *Mater. Sci. Eng. R: Rep.* **2000**, *29*, 1. b) J. H. Li, X. D. Dai, S. H. Liang, K. P. Tai, Y. Kong, B. X. Liu, *Phys. Rep.* **2008**, *455*, 1.
- [4] A. L. Greer, E. Ma, *MRS Bull.* **2007**, *32*, 611.
- [5] W. H. Wang, C. Dong, C. H. Shek, *Mater. Sci. Eng. R: Rep.* **2004**, *44*, 45.
- [6] W. H. Wang, *Prog. Mater. Sci.* **2007**, *52*, 540.
- [7] A. R. Yavari, J. J. Lewandowski, J. Eckert, *MRS Bull.* **2007**, *32*, 635.
- [8] C. A. Schuh, T. C. Hufnagel, U. Ramamurty, *Acta Materialia* **2007**, *55*, 4067.
- [9] M. W. Chen, *Annu. Rev. Mater. Res.* **2008**, *38*, 445.
- [10] a) Y. H. Liu, G. Wang, R. J. Wang, M. X. Pan, W. H. Wang, *Science* **2007**, *315*, 1385. b) J. G. Wang, D. Q. Zhao, M. X. Pan, W. H. Wang, *Appl. Phys. Lett.* **2009**, *94*, 031904. c) P. Yu, Y. H. Liu, G. Wang, H. Y. Bai, W. H. Wang, *J. Mater. Res.* **2007**, *22*, 2384. d) J. G. Wang, D. Q. Zhao, M. X. Pan, W. H. Wang, *Adv. Eng. Mater.* **2008**, *10*, 46. e) P. Yu, W. H. Wang, R. J. Wang, S. X. Lin, X. R. Liu, S. M. Hong, H. Y. Bai, *Appl. Phys. Lett.* **2009**, *94*, 011910. f) P. Yu, H. Y. Bai, J. G. Zhao, C. Q. Jin, W. H. Wang, *Appl. Phys. Lett.* **2007**, *90*, 051906. g) P. Wesseling, T. G. Nieh, W. H. Wang, *Scr. Mater.* **2004**, *51*, 151.
- [11] D. C. Hofmann, J. Y. Suh, A. Wiest, G. Duan, M. Lind, M. D. Demetriou, W. L. Johnson, *Nature* **2008**, *451*, 1085.
- [12] B. Zhang, D. Q. Zhao, W. H. Wang, A. L. Greer, *Phys. Rev. Lett.* **2005**, *94*, 205502.
- [13] a) M. B. Tang, D. Q. Zhao, M. X. Pan, W. H. Wang, *Chin. Phys. Lett.* **2004**, *27*, 901. b) W. H. Wang, J. J. Lewandowski, A. L. Greer, *J. Mater. Res.* **2005**, *20*, 2307. c) Y. D. Dong, W. H. Wang, K. Q. Xiao, L. Liu, S. H. Tong, Y. Z. He, *Mater. Sci. Eng. A* **1991**, *134*, 867.
- [14] Y. Li, S. J. Poon, G. J. Shiflet, J. Xu, D. H. Kim, J. F. Loeffler, *MRS Bull.* **2007**, *32*, 624.
- [15] W. H. Wang, *J. Appl. Phys.* **2006**, *99*, 093506.
- [16] a) B. C. Wei, W. H. Wang, D. Q. Zhao, Y. Zhang, M. X. Pan, B. S. Han, Z. R. Zhang, W. R. Hu, *Phys. Rev. B: Condens. Matter* **2001**, *64*, 012406. b) B. C. Wei, Y. Zhang, Y. X. Zhuang, D. Q. Zhao, M. X. Pan, W. H. Wang, *J. Appl. Phys.* **2001**, *89*, 3529. c) B. C. Wei, W. Löser, L. Xia, S. Roth, M. X. Pan, W. H. Wang, J. Eckert, *Acta Materialia* **2002**, *50*, 4357.
- [17] Z. F. Zhao, Z. Zhang, W. H. Wang, *Appl. Phys. Lett.* **2003**, *82*, 4699.

- [18] a) F. Guo, S. J. Poon, G. Shiflet, *Appl. Phys. Lett.* **2003**, *83*, 2575. b) R. Li, S. Pang, H. Men, C. Ma, T. Zhang, *Scr. Mater.* **2006**, *54*, 1123.
- [19] a) Y. T. Wang, H. Y. Bai, M. X. Pan, D. Q. Zhao, W. H. Wang, *Phys. Rev. B: Condens. Matter* **2006**, *74*, 064422. b) Y. H. Zhao, M. X. Pan, D. Q. Zhao, W. H. Wang, J. Eckert, *J. Phys. D: Appl. Phys.* **2005**, *38*, 2162.
- [20] B. Zhang, M. X. Pan, D. Q. Zhao, W. H. Wang, *Appl. Phys. Lett.* **2004**, *85*, 61.
- [21] a) B. Zhang, W. H. Wang, *Phys. Rev. B: Condens. Matter* **2004**, *70*, 224208. b) B. Zhang, W. H. Wang, *J. Non-Cryst. Solids* **2006**, *352*, 5687.
- [22] B. Zhang, M. X. Pan, D. Q. Zhao, W. H. Wang, *Phys. Rev. B: Condens. Matter* **2006**, *73*, 092201.
- [23] B. Zhang, D. Q. Zhao, M. X. Pan, R. J. Wang, W. H. Wang, *Acta Materialia* **2006**, *54*, 3025.
- [24] B. Zhang, R. J. Wang, W. H. Wang, *Phys. Rev. B: Condens. Matter* **2005**, *72*, 104205.
- [25] S. Li, R. J. Wang, M. X. Pan, D. Q. Zhao, W. H. Wang, *Scr. Mater.* **2005**, *53*, 1489.
- [26] a) S. Li, D. Q. Zhao, M. X. Pan, W. H. Wang, *J. Non-Cryst. Solids* **2005**, *351*, 2568. b) S. Li, R. J. Wang, W. H. Wang, *J. Non-Cryst. Solids* **2006**, *352*, 3942. c) W. H. Wang, P. Wen, X. F. Liu, *J. Non-Cryst. Solids* **2006**, *352*, 5103.
- [27] S. Li, X. K. Xi, Y. X. Wei, Q. Luo, M. B. Tang, B. Zhang, Z. F. Zhao, R. J. Wang, D. Q. Zhao, W. H. Wang, *Sci. Tech. Adv. Mater.* **2005**, *6*, 823.
- [28] S. Li, R. J. Wang, M. X. Pan, D. Q. Zhao, W. H. Wang, *J. Non-Cryst. Solids* **2008**, *354*, 1080.
- [29] S. Li, R. J. Wang, D. Q. Zhao, W. H. Wang, *Intermetallics* **2006**, *14*, 592.
- [30] a) X. K. Xi, S. Li, R. J. Wang, M. X. Pan, D. Q. Zhao, W. H. Wang, *J. Mater. Res.* **2005**, *20*, 2243. b) X. K. Xi, D. Q. Zhao, M. X. Pan, W. H. Wang, *J. Non-Cryst. Solids* **2004**, *344*, 105.
- [31] Y. X. Wei, M. X. Pan, W. H. Wang, *Scr. Mater.* **2006**, *54*, 599.
- [32] Q. Luo, D. Q. Zhao, M. X. Pan, R. J. Wang, W. H. Wang, *Appl. Phys. Lett.* **2006**, *88*, 181909.
- [33] Q. Luo, D. Q. Zhao, M. X. Pan, W. H. Wang, *Appl. Phys. Lett.* **2007**, *90*, 211903.
- [34] Q. Luo, B. Zhang, D. Q. Zhao, M. X. Pan, R. J. Wang, W. H. Wang, *Appl. Phys. Lett.* **2006**, *88*, 151915.
- [35] Q. Luo, D. Q. Zhao, M. X. Pan, W. H. Wang, *Appl. Phys. Lett.* **2006**, *89*, 081914.
- [36] Q. Luo, D. Q. Zhao, M. X. Pan, W. H. Wang, *Appl. Phys. Lett.* **2008**, *92*, 011923.
- [37] H. B. Yu, P. Yu, W. H. Wang, H. Y. Bai, *Appl. Phys. Lett.* **2008**, *92*, 141906.
- [38] Y. T. Wang, Z. Y. Pang, R. J. Wang, D. Q. Zhao, M. X. Pan, B. S. Han, W. L. Wang, W. H. Wang, *J. Non-Cryst. Solids* **2006**, *352*, 444.
- [39] Z. F. Zhao, P. Wen, W. H. Wang, *J. Mater. Res.* **2006**, *21*, 369.
- [40] Z. Li, H. Y. Bai, M. X. Pan, D. Q. Zhao, W. L. Wang, W. H. Wang, *J. Mater. Res.* **2003**, *18*, 2208.
- [41] a) Z. Zhang, D. Q. Zhao, W. H. Wang, *J. Mater. Res.* **2005**, *20*, 314. b) Z. Zhang, L. Xia, R. J. Wang, B. C. Wei, M. X. Pan, W. H. Wang, *Appl. Phys. Lett.* **2002**, *81*, 4371.
- [42] L. Xia, M. B. Tang, H. Xu, M. X. Pan, D. Q. Zhao, W. H. Wang, Y. D. Dong, *J. Mater. Res.* **2004**, *19*, 1307.
- [43] X. F. Liu, R. J. Wang, D. Q. Zhao, M. X. Pan, W. H. Wang, *Appl. Phys. Lett.* **2007**, *91*, 041901.
- [44] Y. T. Wang, X. X. Kui, Y. K. Fang, D. Q. Zhao, M. X. Pan, B. S. Han, W. H. Wang, *Appl. Phys. Lett.* **2004**, *85*, 5989.
- [45] J. P. Chu, C. L. Chiang, H. Wijaya, R. T. Huang, C. W. Wu, B. Zhang, W. H. Wang, T. G. Nieh, *Scr. Mater.* **2006**, *55*, 227.
- [46] D. Chen, A. Takeuchi, A. Inoue, *Mater. Sci. Eng. A* **2007**, *457*, 226.
- [47] W. H. Li, K. Shin, C. G. Lee, B. C. Wei, *Appl. Phys. Lett.* **2007**, *90*, 171928.
- [48] A. A. Kundig, T. Schweizer, E. Schafner, J. F. Löffler, *Scr. Mater.* **2007**, *56*, 289.
- [49] Q. K. Jiang, G. Q. Zhang, L. Yang, X. D. Wang, K. Saks, H. Franz, R. Wunderlich, H. Fecht, J. Z. Jiang, *Acta Materialia* **2007**, *55*, 4409.
- [50] M. B. Tang, H. Y. Bai, W. H. Wang, D. Bogdanov, K. Winzer, K. Samwer, T. Egami, *Phys. Rev. B: Condens. Matter* **2007**, *75*, 172201.
- [51] Y. T. Wang, H. Y. Bai, M. X. Pan, D. Q. Zhao, W. H. Wang, *Sci. China G: Phys. Mech. Astronomy* **2008**, *51*, 337.
- [52] H. B. Yu, P. Yu, H. Y. Bai, *J. Non-Cryst. Solids* **2008**, *354*, 4539.
- [53] B. Zhang, H. Y. Bai, R. J. Wang, Y. Wu, W. H. Wang, *Phys. Rev. B: Condens. Matter* **2007**, *76*, 012201.
- [54] P. Yu, R. J. Wang, D. Q. Zhao, H. Y. Bai, *Appl. Phys. Lett.* **2007**, *91*, 201911.
- [55] a) M. B. Tang, H. Y. Bai, M. X. Pan, D. Q. Zhao, W. H. Wang, *J. Non-Cryst. Solids* **2005**, *351*, 2572. b) Y. Li, H. Y. Bai, P. Wen, Z. X. Liu, Z. F. Zhao, *J. Phys. C: Solid State Phys.* **2003**, *15*, 4809.
- [56] J. Q. Wang, W. H. Wang, H. Y. Bai, *Appl. Phys. Lett.* **2009**, *94*, 041910.
- [57] D. Turnbull, *Contemp. Phys.* **1969**, *10*, 437.
- [58] Z. P. Lu, C. T. Liu, *Phys. Rev. Lett.* **2003**, *91*, 115503.
- [59] Y. Zhang, D. Q. Zhao, W. H. Wang, *J. Non-Cryst. Solids* **2003**, *315*, 206.
- [60] T. Egami, *Mater. Sci. Eng. A* **1997**, *226–228*, 261.
- [61] a) X. F. Bian, J. Guo, *Appl. Phys. Lett.* **2007**, *91*, 221910. b) L. Xia, W. H. Li, S. S. Fang, B. C. Wei, Y. D. Dong, *J. Appl. Phys.* **2006**, *99*, 026103. c) Z. Z. Yuan, S. L. Bao, Y. Lu, D. P. Zhang, L. Yao, *J. Alloys Compd.* **2008**, *459*, 251. d) Y. M. Wang, J. B. Qiang, C. H. Chong, C. H. Shek, *J. Mater. Res.* **2003**, *18*, 642.
- [62] A. H. Cai, *Appl. Phys. Lett.* **2008**, *92*, 111909.
- [63] J. C. Dyre, *Rev. Mod. Phys.* **2006**, *78*, 953.
- [64] J. J. Lewandowski, W. H. Wang, A. L. Greer, *Philos. Mag. Lett.* **2005**, *85*, 77.
- [65] W. L. Johnson, K. Samwer, *Phys. Rev. Lett.* **2005**, *95*, 195501.
- [66] a) W. H. Wang, *J. Non-Cryst. Solids* **2005**, *351*, 1481. b) W. H. Wang, P. Wen, *J. Mater. Res.* **2003**, *18*, 2747.
- [67] a) X. K. Xi, L. L. Li, B. Zhang, W. H. Wang, Y. Wu, *Phys. Rev. Lett.* **2007**, *99*, 095501. b) X. K. Xi, D. Q. Zhao, M. X. Pan, W. H. Wang, Y. Wu, J. J. Lewandowski, *Phys. Rev. Lett.* **2005**, *94*, 125510. c) G. Wang, D. Q. Zhao, H. Y. Bai, M. X. Pan, A. L. Xia, B. S. Han, X. K. Xi, Y. Wu, W. H. Wang, *Phys. Rev. Lett.* **2007**, *98*, 235501. d) G. Wang, Y. T. Wang, Y. H. Liu, M. X. Pan, D. Q. Zhao, W. H. Wang, *Appl. Phys. Lett.* **2006**, *89*, 121909. e) X. K. Xi, D. Q. Zhao, M. X. Pan, W. H. Wang, Y. Wu, J. J. Lewandowski, *Appl. Phys. Lett.* **2006**, *89*, 181911.
- [68] V. N. Novikov, A. P. Sokolov, *Phys. Rev. B: Condens. Matter* **2006**, *74*, 064203.
- [69] M. Jiang, L. Dai, *Phys. Rev. B: Condens. Matter* **2007**, *76*, 093506.
- [70] T. Scopigno, G. Ruocco, F. Sette, G. Monaco, *Science* **2003**, *302*, 849.
- [71] O. N. Senkov, *Phys. Rev. B: Condens. Matter* **2007**, *76*, 104202.
- [72] Y. Li, H. Y. Bai, W. H. Wang, K. Samwer, *Phys. Rev. B: Condens. Matter* **2006**, *74*, 052201.
- [73] B. Yang, C. T. Liu, T. G. Nieh, *Appl. Phys. Lett.* **2006**, *88*, 221911.
- [74] H. S. Chen, J. T. Krause, *Scr. Metall.* **1977**, *11*, 761.
- [75] a) W. H. Wang, M. P. Macht, H. Wollenberger, *Appl. Phys. Lett.* **1997**, *71*, 58. b) W. H. Wang, Z. Bian, Y. Zhang, M. X. Pan, D. Q. Zhao, *Intermetallics* **2002**, *10*, 1249. c) W. H. Wang, Q. Wei, M. P. Macht, H. Wollenberger, *Appl. Phys. Lett.* **1997**, *71*, 1053.
- [76] J. Q. Wang, W. H. Wang, H. Y. Bai, unpublished.
- [77] a) W. H. Wang, H. Y. Bai, *J. Appl. Phys.* **1998**, *84*, 5961. b) W. H. Wang, M. X. Pan, D. Q. Zhao, Y. Hu, H. Y. Bai, *J. Phys.: Condens. Matter* **2004**, *16*, 3719. c) W. H. Wang, Q. Wei, S. Friedrich, *Phys. Rev. B: Condens. Matter* **1998**, *57*, 8211. d) W. H. Wang, D. Q. Zhao, D. W. He, Y. S. Yao, *Appl. Phys. Lett.* **1999**, *75*, 2770. e) W. H. Wang, H. Y. Bai, M. Zhang, J. H. Zhao, X. Y. Zhang, W. K. Wang, *Phys. Rev. B: Condens. Matter* **1999**, *59*, 10811. f) W. H. Wang, Z. X. Bao, J. Eckert, *Phys. Rev. B: Condens. Matter* **2000**, *61*, 3166.
- [78] S. Schneider, A. Bracchi, K. Samwer, M. Seibt, P. Thiyagarajan, *Appl. Phys. Lett.* **2002**, *80*, 1749.
- [79] A. Bracchi, K. Samwer, S. Schneider, J. F. Löffler, *Appl. Phys. Lett.* **2003**, *82*, 721.
- [80] N. H. Dan, N. X. Phuc, N. M. Hong, J. Ding, D. Givord, *J. Magn. Magn. Mater.* **2001**, *226*, 1385.
- [81] D. Triyono, R. Sato Turtelli, R. Grössinger, H. Michor, K. R. Pirota, M. Knobel, H. Sassik, T. Mathias, S. Höfner, J. Fidler, *J. Magn. Magn. Mater.* **2001**, *242–245*, 1321.

- [82] R. Sato Turtelli, D. Triyono, R. Grössinger, H. Michor, J. H. Espina, J. P. Sinnecker, H. Sassik, J. Eckert, G. Kumar, Z. Sun, G. J. Fan, *Phys. Rev. B: Condens. Matter* **2007**, *66*, 054441.
- [83] Z. G. Sun, W. Löser, J. Eckert, K.-H. Müller, L. Schultz, *J. Appl. Phys.* **2002**, *91*, 9267.
- [84] O. Tegus, E. Bruck, K. H. J. Buschow, F. R. de Boer, *Nature* **2002**, *415*, 150.
- [85] V. Provenzano, A. J. Shapiro, R. D. Shull, *Nature* **2004**, *429*, 853.
- [86] Z. B. Guo, Y. W. Du, H. Huang, D. Feng, *Phys. Rev. Lett.* **1997**, *78*, 1142.
- [87] T. D. Shen, R. B. Schwarz, J. Y. Coulter, J. D. Thompson, *J. Appl. Phys.* **2002**, *91*, 5240.
- [88] X. Bohigas, J. Tejada, A. del Moral, *Appl. Phys. Lett.* **2002**, *81*, 2427.
- [89] P. J. von Ranke, V. K. Pecharsky, K. A. Gschneidner, *Phys. Rev. B: Condens. Matter* **1998**, *58*, 12110.
- [90] V. Franco, J. S. Blázquez, A. Conde, *Appl. Phys. Lett.* **2006**, *88*, 042505.
- [91] H. Fu, X. T. Zu, H. J. Yu, B. H. Teng, X. T. Zu, *Solid State Commun.* **2008**, *145*, 15.
- [92] L. Liang, X. Hui, G. L. Chen, *Mater. Sci. Eng. A* **2008**, *147*, 13.
- [93] J. Du, Q. Zheng, E. Brück, K. H. J. Buschow, W. B. Cui, W. J. Feng, Z. D. Zhang, *J. Magn. Magn. Mater.* **2009**, *321*, 41.
- [94] G. S. Burkhanov, O. D. Chistyakov, *Sov. Tech. Phys. Lett.* **1991**, *17*, 353.
- [95] K. Binder, A. P. Young, *Rev. Mod. Phys.* **1986**, *58*, 801.
- [96] R. Fisch, *Phys. Rev. B: Condens. Matter* **1990**, *42*, 540.
- [97] J. Dho, W. S. Kim, N. H. Hur, *Phys. Rev. Lett.* **2002**, *89*, 027202.
- [98] J. R. L. de Almeida, D. J. Thouless, *J. Phys. A* **1978**, *11*, 983.
- [99] G. R. Stewart, *Rev. Mod. Phys.* **2006**, *78*, 743.
- [100] E. Miranda, V. Dobrosavljevic, G. Kotliar, *Phys. Rev. Lett.* **1997**, *78*, 290.
- [101] A. H. Castro Neto, B. A. Jones, *Phys. Rev. B: Condens. Matter* **2000**, *62*, 14975.
- [102] H. S. Chen, J. T. Krause, E. Coleman, *J. Non-Cryst. Solids* **1975**, *18*, 157.
- [103] Y. Zhang, D. Q. Zhao, R. J. Wang, W. H. Wang, *Acta Materialia* **2003**, *51*, 1971.
- [104] a) W. H. Wang, R. J. Wang, F. Y. Li, D. Q. Zhao, M. X. Pan, *Appl. Phys. Lett.* **1999**, *74*, 1803. b) W. H. Wang, H. Y. Bai, J. L. Luo, R. J. Wang, D. Jin, *Phys. Rev. B: Condens. Matter* **2000**, *62*, 25.
- [105] L. M. Wang, W. H. Wang, R. J. Wang, *Appl. Phys. Lett.* **2000**, *77*, 1147.
- [106] L. M. Wang, W. H. Wang, W. K. Wang, *Appl. Phys. Lett.* **2000**, *77*, 3734.
- [107] W. H. Wang, P. Wen, M. X. Pan, R. J. Wang, *Appl. Phys. Lett.* **2001**, *79*, 3947.
- [108] W. H. Wang, R. J. Wang, W. T. Yang, B. C. Wei, P. Wen, D. Q. Zhao, M. X. Pan, *J. Mater. Res.* **2002**, *17*, 1385.
- [109] P. Wen, R. J. Wang, W. H. Wang, *J. Mater. Res.* **2002**, *17*, 1785.
- [110] R. J. Wang, W. H. Wang, F. Y. Li, L. M. Wang, *J. Phys. C: Solid State Phys.* **2003**, *15*, 603.
- [111] a) Z. Bian, R. J. Wang, M. X. Pan, W. H. Wang, *Adv. Mater.* **2003**, *15*, 616. b) Z. Bian, R. J. Wang, W. H. Wang, T. Zhang, A. Inoue, *Adv. Funct. Mater.* **2004**, *14*, 55. c) Z. Bian, M. X. Pan, Y. Zhang, W. H. Wang, *Appl. Phys. Lett.* **2002**, *81*, 4739.
- [112] Z. Zhang, R. J. Wang, M. X. Pan, W. H. Wang, *J. Phys. C: Solid State Phys.* **2003**, *15*, 4503.
- [113] D. E. Gray, *American Institute of Physics Handbook*, 3rd ed., McGraw-Hill, New York **1973**, Ch.3.
- [114] W. H. Wang, D. Q. Zhao, M. X. Pan, P. Wen, *J. Mater. Res.* **2003**, *18*, 2747.
- [115] W. H. Wang, F. Y. Li, M. X. Pang, D. Q. Zhao, R. J. Wang, *Acta Materialia* **2004**, *52*, 715.
- [116] M. L. Lind, G. Duan, W. L. Johnson, *Phys. Rev. Lett.* **2006**, *97*, 015501.
- [117] E. F. Lambson, W. A. Lambson, J. E. MacDonald, M. R. J. Gibbs, G. A. Saunders, D. Turnbull, *Phys. Rev. B: Condens. Matter* **1986**, *33*, 2380.
- [118] P. Yu, R. J. Wang, D. Q. Zhao, H. Y. Bai, *Appl. Phys. Lett.* **2007**, *90*, 251904.
- [119] R. J. Wang, F. Y. Li, J. F. Wang, W. H. Wang, *Appl. Phys. Lett.* **2003**, *83*, 2814.
- [120] F. D. Murnaghan, *Proc. Natl. Acad. Sci. USA* **1944**, *30*, 244.
- [121] S. Sen, S. Gaudio, B. G. Aitken, C. E. Lesher, *Phys. Rev. Lett.* **2006**, *97*, 025504.
- [122] Y. Katayama, T. Mizutani, W. Utsumi, O. Shimomura, M. Yamakata, K. Funakoshi, *Nature* **2000**, *403*, 170.
- [123] H. W. Sheng, H. Z. Liu, Y. Q. Cheng, J. Wen, P. L. Lee, W. K. Luo, S. D. Shastri, E. Ma, *Nat. Mater.* **2007**, *6*, 192.
- [124] Q. S. Zeng, Y. C. Li, C. M. Feng, P. Liermann, M. Somayazulu, H. K. Mao, R. Yang, J. Z. Jiang, *Proc. Natl. Acad. Sci. USA* **2007**, *104*, 13565.
- [125] X. R. Liu, S. M. Hong, *Appl. Phys. Lett.* **2006**, *88*, 042505.
- [126] a) J. F. Li, D. Q. Zhao, M. L. Zhang, W. H. Wang, *Appl. Phys. Lett.* **2008**, *93*, 171907. b) P. Yu, W. H. Wang, S. M. Hong, H. Y. Bai, *Appl. Phys. Lett.* **2009**, *94*, 011910.
- [127] P. X. Ma, *Mater. Today* **2004**, *7*, 30.
- [128] R. D. Conner, H. Choi-Yim, W. L. Johnson, *J. Mater. Res.* **1999**, *14*, 3292.
- [129] M. M. Trancy, T. W. Ebbesen, J. M. Gibson, *Nature (London)* **1996**, *381*, 678.
- [130] J. R. Heath, *Acc. Chem. Res.* **1999**, *32*, 388.
- [131] C. R. Martin, *Science* **1994**, *266*, 1961.
- [132] T. S. Ahmadi, Z. L. Wang, T. C. Green, A. Henglein, M. A. El-Sayed, *Science* **1996**, *272*, 1924.
- [133] S. J. A. Koh, H. P. Lee, C. Lu, Q. H. Cheng, *Phys. Rev. B: Condens. Matter* **2005**, *72*, 085414.
- [134] K. S. Nakayama, Y. Yokoyama, G. Xie, Q. S. Zhang, M. W. Chen, T. Sakurai, A. Inoue, *Nano Lett.* **2008**, *8*, 516.
- [135] *The Physics of Strength and Plasticity* (Ed: A. S. Argon), MIT Press, Cambridge MA **1969**.
- [136] X. X. Xia, W. H. Wang, A. L. Greer, *J. Mater. Res.* **2009**, in press.
- [137] H. L. Ewalds, R. J. H. Wanhill, *Fracture Mechanics 56–63*, Edward Arnold, London **1984**.
- [138] J. J. Lewandowski, A. L. Greer, *Nat. Mater.* **2006**, *5*, 15.
- [139] K. Zhao, K. S. Liu, J. F. Li, W. H. Wang, L. Jiang, *Scr. Mater.* **2009**, *60*, 225.
- [140] A. Zaluska, L. Zaluski, J. O. Strom-Olsen, *J. Alloys Compd.* **2000**, *307*, 157.
- [141] H. Y. Erbil, A. L. Demirel, Y. Avci, O. Mert, *Science* **2003**, *299*, 1377.
- [142] W. Barthlott, C. Neinhuis, *Planta* **1997**, *202*, 1.
- [143] a) X. J. Feng, L. Jiang, *Adv. Mater.* **2006**, *18*, 3063. b) J. Genzer, K. Efimenko, *Biofouling* **2006**, *22*, 339. c) P. Roach, N. J. Shirtcliffe, M. I. Newton, *Soft Matter* **2008**, *4*, 224. d) G. Palasantzas, J. T. M. de Hosson, *Acta Materialia* **2000**, *48*, 3641.
- [144] A. L. Greer, *Mater. Today* **2009**, *12*, 14.
- [145] D. Ma, A. D. Stoica, X. L. Wang, *Nat. Mater.* **2008**, *8*, 30.
- [146] D. Pan, A. Inoue, T. Sakurai, M. W. Chen, *Proc. Natl. Acad. Sci. USA* **2008**, *105*, 14769.
- [147] X. P. Tang, U. Geyer, R. Busch, W. L. Johnson, Y. Wu, *Nature* **1999**, *402*, 160.
- [148] T. Egami, *J. Alloy Compd.* **2007**, *434–435*, 110.